

Continuous carbon nanotube fiber with an extremely high average specific strength of 4.1 N/tex

Yutao Niu^{1,2,3,§}, Zhao He^{3,4,§}, Shan Wang^{3,5,§}, Yichi Zhang^{1,2,3}, Zhengpeng Yang⁵, Yongyi Zhang^{1,2,3(✉)}, Zhenzhong Yong^{1,2,3}, Kunjie Wu^{2,3}, Liming Zhao^{2(✉)}, Zhanhu Guo^{6(✉)}, Muqiang Jian^{7(✉)}, Qingwen Li^{1,2(✉)}

¹ School of Nano-Tech and Nano-Bionics, University of Science and Technology of China, Hefei 230026, China

² Key Laboratory of Multifunctional Nanomaterials and Smart Systems, Suzhou Institute of Nano-Tech and Nano-Bionics, Chinese Academy of Sciences, Suzhou 215123, China

³ Division of Nanomaterials and Jiangxi Key Lab of Carbonene Materials, Jiangxi Institute of Nanotechnology, Nanchang 330200, China

⁴ College of Chemistry and Chemical Engineering/Film Energy Chemistry for Jiangxi Provincial Key Laboratory (FEC), Nanchang University, 999 Xuefu Avenue, Nanchang 330031, China

⁵ Henan Key Laboratory of Materials on Deep-Earth Engineering, School of Materials Science and Engineering, Henan Polytechnic University, Jiaozuo 454003, China

⁶ Integrated Composites Lab, Department of Mechanical and Construction Engineering, Northumbria University, Newcastle Upon Tyne NE1 8ST, UK

⁷ Beijing Graphene Institute (BGI), Beijing 100095, China

§ Yutao Niu, Zhao He, and Shan Wang contributed equally to this work.

Nano Res., Just Accepted Manuscript • <https://doi.org/10.26599/NR.2025.94907584>

<https://www.scipen.com/journal/1998-0124> on May. 14, 2025

© The Author(s)

Just Accepted

This is a “Just Accepted” manuscript, which has been examined by the peer-review process and has been accepted for publication. A “Just Accepted” manuscript is published online shortly after its acceptance, which is prior to technical editing and formatting and author proofing. Tsinghua University Press (TUP) provides “Just Accepted” as an optional and free service which allows authors to make their results available to the research community as soon as possible after acceptance. After a manuscript has been technically edited and formatted, and the page proofs have been corrected, it will be removed from the “Just Accepted” web site and published officially with volume and article number (e.g., *Nano Research*, 2025, 18, 94906990). Please note that technical editing may introduce minor changes to the manuscript text and/or graphics which may affect the content, and all legal disclaimers that apply to the journal pertain. In no event shall TUP be held responsible for errors or consequences arising from the use of any information contained in these “Just Accepted” manuscripts. To cite this manuscript please use its Digital Object Identifier (DOI®), which is identical for all formats of publication.

Research Article

Continuous carbon nanotube fiber with an extremely high average specific strength of 4.1 N/tex

Yutao Niu^{1,2,3,§}, Zhao He^{3,4,§}, Shan Wang^{3,5,§}, Yichi Zhang^{1,2,3}, Zhengpeng Yang⁵, Yongyi Zhang^{1,2,3,*}, Zhenzhong Yong^{1,2,3}, Kunjie Wu^{2,3}, Liming Zhao^{2,*}, Zhanhu Guo^{6,*}, Muqiang Jian^{7,*}, and Qingwen Li^{1,2,*}

¹ School of Nano-Tech and Nano-Bionics, University of Science and Technology of China, Hefei 230026, China

² Key Laboratory of Multifunctional Nanomaterials and Smart Systems, Suzhou Institute of Nano-Tech and Nano-Bionics, Chinese Academy of Sciences, Suzhou 215123, China

³ Division of Nanomaterials and Jiangxi Key Lab of Carbonene Materials, Jiangxi Institute of Nanotechnology, Nanchang 330200, China

⁴ College of Chemistry and Chemical Engineering/Film Energy Chemistry for Jiangxi Provincial Key Laboratory (FEC), Nanchang University, 999 Xuefu Avenue, Nanchang 330031, China

⁵ Henan Key Laboratory of Materials on Deep-Earth Engineering, School of Materials Science and Engineering, Henan Polytechnic University, Jiaozuo 454003, China

⁶ Integrated Composites Lab, Department of Mechanical and Construction Engineering, Northumbria University, Newcastle Upon Tyne NE1 8ST, UK

⁷ Beijing Graphene Institute (BGI), Beijing 100095, China

© The Author(s) 2025

Received: 21 March 2025; Revised: 11 May 2025; Accepted: 14 May 2025

✉Address correspondence to Yongyi Zhang, yyzhang2011@sinano.ac.cn; Liming Zhao, lmzhao2019@sinano.ac.cn; Zhanhu Guo, zhanhu.guo@northumbria.ac.uk; Muqiang Jian, jianmqcnc@pku.edu.cn; Qingwen Li, qwli2007@sinano.ac.cn

Cite this article: Nano Research, 2025, 18, 94907584.

<https://doi.org/10.26599/NR.2025.94907584>

Just Accepted

Abstract

Carbon nanotube fibers (CNTFs), which hold a transformative potential across fields from aerospace to wearable electronics, have been reported as superstrong fibers, while the fabrication of continuous fibers with excellent strength remains a challenge. Herein, we proposed a mixed carbon-source strategy that engineered carbon nanotube (CNT) aerogels with optimally aligned and controlled-entanglement CNT bundles, ensuring structural uniformity and enabling densification into highly oriented architectures via chlorosulfonic acid-assisted stretching, thus yielding continuous high-performance CNTFs. These continuous CNTFs exhibited superior tensile strength ($4.10 \pm 0.17 \text{ N tex}^{-1}$, exceeding T1100), modulus ($268 \pm 16 \text{ N tex}^{-1}$, 1.4 times of T1100), thermal conductivity ($400 \text{ W m}^{-1} \text{ K}^{-1}$, over 30 times of T1100) and electrical conductivity ($1480 \text{ S m}^2 \text{ kg}^{-1}$), along with exceptional flexibility indicated by knot-strength retention exceeding 45%. Comprehensive multi-point assessments confirmed that this method yielded a remarkable uniformity in both structural and functional properties across kilometer-scale lengths. These findings highlight the crucial role of nanotube alignment and interfacial engineering in enabling the scalable industrial implementation of high-performance CNTFs.

Keywords: Continuous carbon nanotube fibers; High strength; Thermal conductivity; Structural regulation; Carbon source.

1. Introduction

Carbon nanotube fibers (CNTFs) have recently emerged as a novel category of high-performance carbon-based fibers, presenting a significant potential as integrated structural-functional materials, and more importantly featuring remarkable structural strength, flexibility and electrical conductivity [1-4]. Recently, Wei et al. have witnessed that individual CNT can achieve a dynamic mechanical strength over 90 GPa, and the tensile strength of CNT bundles can reach as high as 80 GPa [5, 6]. In the case of short-length macroscopic CNTFs, a specific strength over 9 N tex⁻¹ can be available to the fiber generated by floating catalyst chemical vapor deposition (FCCVD) method [7], and the mechanical strength of the fiber derived from wet spinning can climb up to 6.74 GPa [8]. Compared to wet spinning techniques, FCCVD allows for the generation of significantly elongated CNTs within fiber architectures, typically by an order of magnitude [9-11]. From a microstructural standpoint, elongated CNTs inherently enhance load transfer efficiency and mitigate stress concentrations under mechanical loading, theoretically imparting fibers with elevated mechanical performance [12, 13]. Nonetheless, CNTFs directly fabricated via FCCVD have not distinctly surpassed wet-spun fibers in terms of mechanical performance [14-16]. This phenomenon primarily arises from current limitations in the FCCVD fabrication process, especially structural imperfections during CNT assembly, resulting in a relatively low degree of CNT alignment within fibers [17]. The resultant misalignment and disordered arrangement of CNTs within FCCVD-derived fibers markedly impede efficient inter-tube load transfer under applied stress, thereby significantly constraining the full realization of their intrinsic mechanical attributes [18].

To overcome intrinsic structural limitations and further enhance mechanical performance, researchers have predominantly focused on structural optimization along three key dimensions [19]. Firstly, based on the concept of control proposed by Vilatela, improving CNT alignment within fibers ensures concurrent load-bearing engagement of all CNTs under tensile stress, effectively minimizing stress concentrations and fully exploiting its intrinsic high-strength characteristics [20]. Secondly, densification strategies aim to amplify inter-tube contact area, reducing energy dissipation associated with void spaces and consequently improving load transfer efficiency among CNTs without altering inter-tube interaction strength [21]. Through mechanical roller-densification technology, Li et al. successfully elevated the mechanical strength of carbon nanotube fibers from 5.7 GPa to 7.67 GPa by optimized rolling process [22]. Thirdly, strengthening inter-tube interactions transforms relatively weak van der Waals forces between CNT bundles into stronger chemical interactions, significantly enhancing cohesive strength and facilitating synergistic mechanical performance under stress conditions [23, 24]. Zhang et al. achieved a 14 GPa dynamic strength in composite fibers through interfacial engineering leveraging PBO nanofibers to strengthen inter-tube interactions within CNT architectures [25]. Guided by these core principles, various post-processing techniques, including twisting[17], roller compaction densification [26], inter-tube crosslinking [27] and drawing [28], have been developed. Notably, the chlorosulfonic acid (CSA)-assisted drawing approach has demonstrated considerable efficacy by simultaneously optimizing CNT orientation and enhancing inter-tube contact [29]. However, current researches employing this method predominantly focus on short-length fiber processing, and the report on long-length fiber is rare [30]. This

limitation primarily arises due to the heterogeneous nature of high-strength original CNT fibers fabricated via FCCVD, complicating the uniform application of post-processing treatments and thereby increasing the propensity for fiber breakage. Consequently, fabricating high-strength and uniform original fibers emerges as an essential prerequisite for enabling continuous and effective fiber processing.

The carbon source utilized during FCCVD exerts substantial influence on the gas-phase CNT assembly structure. Herein, an innovative mixed carbon source strategy by incorporating a minor quantity of ethanol into an acetone-based carbon source was put forward, yielding CNT aerogels with predominantly aligned networks interspersed with limited entangled structures. Such entangled structures provided critical structural integrity and uniformity to the aerogel, while the aligned network promoted the formation of large, highly efficient load-bearing CNT bundles following fiberization. Consequently, the resulting pristine CNTFs (P-CNTFs) delivered exceptional strength coupled with remarkable homogeneity. After undergoing continuous CSA-assisted drawing, CSA-enhanced CNTFs (CSA-CNTFs) achieved kilometer-scale fabrication with a tensile specific strength of 4.1 N tex^{-1} (exceeding T1100), specific modulus of 268 N tex^{-1} (1.4 times of T1100), thermal conductivity of $400 \text{ W m}^{-1} \text{ K}^{-1}$ (over 30 times of T1100) and electrical conductivity of $1480 \text{ S m}^2 \text{ K}^{-1}$, while maintaining consistently stable performance. Furthermore, CSA-CNTFs demonstrated outstanding flexibility, retaining knot strength at levels exceeding 45% of their initial tensile strength, thereby establishing a solid foundation for practical implementation in advanced high-performance CNTF applications.

2. Experimental section

2.1 Materials.

Acetone (99.5%) and ethanol (99.5%) were procured from

Sinopharm Chemical Reagent Co., Ltd. Ferrocene and thiophene were acquired from Shanghai Aladdin Biochemical Technology Co., Ltd. All chemical reagents were utilized as received, without any additional purification procedures.

2.2 Synthesis of P-CNTFs. P-CNTFs were synthesized using the FCCVD direct spinning method. A precursor solution containing liquid carbon source (either ethanol or acetone), ferrocene, thiophene and water was delivered uniformly into a high-temperature ceramic reactor via a hydrogen-argon gas mixture at a total flow rate of 5 L min^{-1} . The growth of CNTs was facilitated at 1300°C , forming aerogel-like CNT networks. These networks contracted and densified into wet CNTFs after traversing a water bath, and were subsequently collected onto a rotating bobbin with winding speeds between 4 and 24 m min^{-1} . Finally, the wet CNTFs underwent roll-to-roll drying at 400°C to produce the P-CNTFs.

2.3 Synthesis of CSA-CNTFs. Post-processing of as-grown P-CNTFs into CSA-CNTFs involved a meticulously designed sequence comprising unwinding, stretching, solvent exchange, annealing and winding steps. Initially, P-CNTFs were actively unwound using a motor-driven unwinding apparatus and immersed into a CSA-assisted stretching unit, inducing protonation-driven fiber swelling that facilitated efficient stretching. Following this stage, fibers underwent solvent treatment in baths containing dichloromethane or acetone, effectively extracting residual protonation acids and enabling fiber reshaping. Subsequently, reshaped fibers were subjected sequentially to annealing processes conducted at temperatures of 250°C and 350°C within tubular furnaces. This annealing step served dual purposes: it eliminated residual substances entrapped within the fiber matrix and concurrently mitigated internal stresses, thereby significantly enhancing fiber densification and

structural integrity. The final CSA-CNTFs were then systematically collected at the winding unit. Precise control over the stretching ratio was maintained by adjusting the speed differential between the winding and unwinding motors. The entire process from protonation acid immersion to final fibers annealing was strictly maintained within an inert gas atmosphere to prevent undesired interactions.

2.4 Characterization. The microstructural characteristics of CNT networks and CNTFs were investigated utilizing scanning electron microscopy (SEM, Thermo Fisher Scientific Apero C HiVac) and transmission electron microscopy (TEM, FEI Talos F200X). Cross-sectional morphology was examined following precise sample preparation using a focused ion beam (FIB, FEI Helios NanoLab 600i). CNTF orientation was quantitatively assessed by wide-angle X-ray scattering (WAXS, Xeuss 3.0), with data processing conducted via Foxtrot software. Orientation degree (S) was calculated based on the full width at half maximum (FWHM) extracted from azimuthal integration of the WAXS patterns, according to the following Eq. (1):

$$S = (180 - FWHM)/180 \quad (1)$$

Mechanical properties were evaluated through tensile testing using an MTS E43 fiber-testing system equipped with a 10 N load cell. CNTF samples were securely clamped with an initial gauge length of 10 mm and subjected to tensile loading at a displacement rate of 1 mm min^{-1} . Linear density (D) measurements of CNTFs were obtained by weighing a known fiber length and calculated using Eq. (2):

$$D = W/L \quad (2)$$

where D (tex) represents linear density, W (g) is fiber weight, and L (km) corresponds to fiber length. For accuracy, fibers of 5 m in length were weighed on a microbalance (Mettler Toledo XPR2U). Electrical measurements were carried out using a four-point

probe resistance meter (HIOKI RM 3544) at room temperature. The thermal conductivity of composite phase change fibers was evaluated using the 3ω harmonic method.

3. Results and discussion

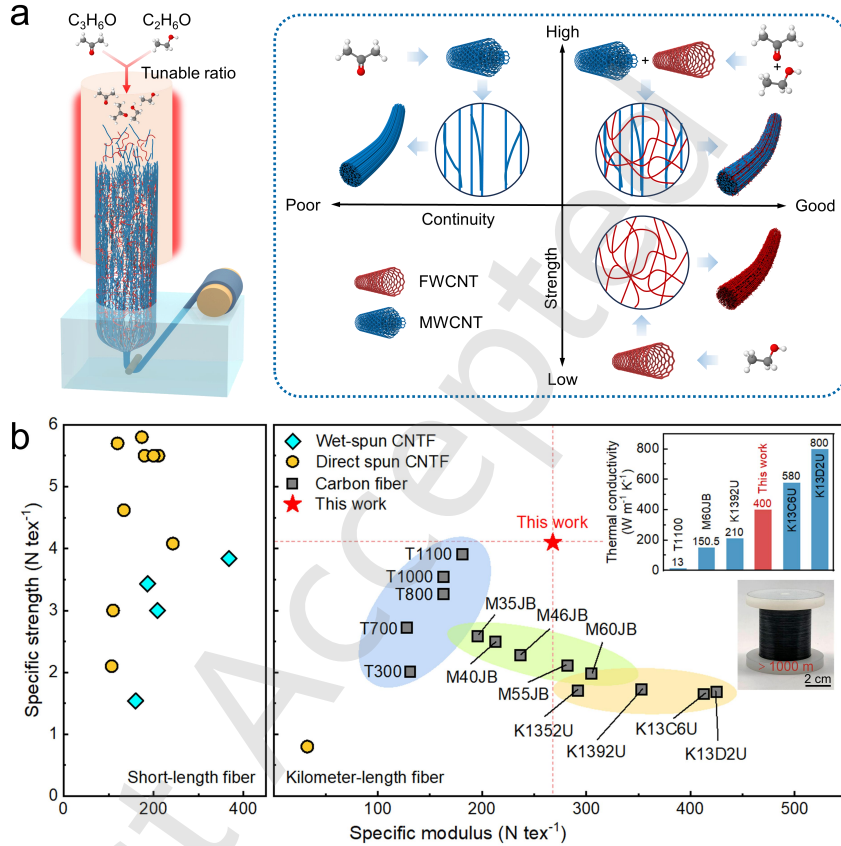


Figure 1 Fabrication of scalable CNTFs. (a) Manufacturing procedure and assembly principle. (b) Comparison of mechanical performance and thermal conductivity with previously reported CNTFs and commercial carbon fibers.

Achieving continuous P-CNTFs with both high strength and excellent uniformity is essential for the further enhancement of CNTF properties via post-processing techniques. Prior investigations have established that P-CNTFs synthesized from an acetone-based carbon source exhibit superior mechanical strength due to the

formation of highly aligned CNT bundles within the sheath structure [31], but the pronounced variability in mechanical performance suggests inherent structural heterogeneity with localized imperfections disrupting uniformity. To address the persistent challenge of simultaneously enhancing both strength and uniformity in P-CNTFs derived from single-carbon-source systems, this work proposed a mixed carbon-source FCCVD synthesis strategy, grounded in prior findings on the regulatory influence of carbon sources on CNT growth. As illustrated in Figs. 1 and S1, employing a tunable acetone-ethanol mixture as the feedstock yielded an aerogel structure featuring cross-linked multi-walled carbon nanotubes (MWCNTs) and few-walled carbon nanotubes (FWCNTs). Also, precise modulation of morphological and assembly behaviors ensured uniform load distribution among the CNT assemblies during fiber formation. Consequently, P-CNTFs exhibiting simultaneously enhanced mechanical strength and exceptional uniformity were produced. The well-defined uniformity of the fiber structure enabled efficient CSA-assisted continuous stretching, allowing the fabrication of kilometer-scale CSA-CNTFs. This advancement marked a crucial transition from localized fiber processing to large-scale continuous production of high-performance CNTFs. The specific strength and modulus of our CNTFs surpass that of commercially available T1100 carbon fiber, and the thermal conductivity is over 30 times that of T1100. (Fig. 1b; Table S1 and S2).

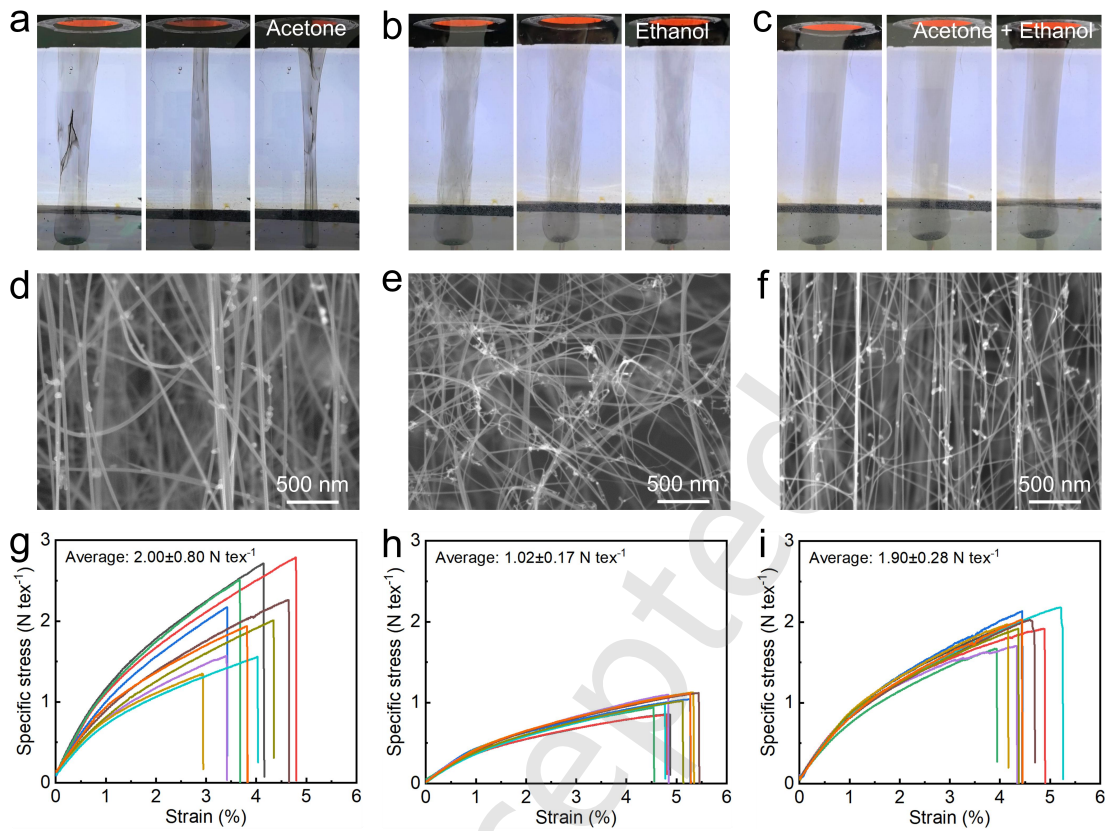


Figure 2 Morphological and mechanical characterizations of P-CNTFs derived from different carbon sources. Photographs and SEM images of CNT aerogels grown from acetone (a,d), ethanol (b,e) and acetone-ethanol mixture (c,f). Stress-strain curves of P-CNTFs derived from acetone (g), ethanol (h) and acetone-ethanol (i) carbon sources.

Based on comprehensive macroscopic and microscopic analysis of CNT aerogel assemblies, we elucidated the influence of carbon sources on fiber homogeneity and underlying mechanism through the following contents. Structural integrity of CNT aerogels, as precursors for fiber formation, critically determined the final fiber performance. In acetone-derived systems, aerogels exhibited apparent structural defects during continuous synthesis, manifesting macroscopically as localized sheath ruptures, visible black agglomerates, and extensive fractures (Fig. 2a). These black

agglomerates consisted predominantly of densely aggregated carbon nanofiber (Fig. S2), subsequently leading to compositional heterogeneity (Fig. S3a) and significant mechanical performance fluctuations (Figs. 2g and S4a). Such defects originated from turbulent instabilities induced by the low-temperature carrier gas and liquid carbon source injection within the FCCVD reactor, causing erratic aerogel oscillations and collisions with the reactor wall. Due to the predominantly straight and aligned MWCNT bundles within the acetone-based aerogel (Figs. 2d and S5a-c), weak inter-tube van der Waals interactions failed to withstand localized stress concentrations [32], initiating localized fractures and abrupt diameter reduction upon collision. Subsequently, aerogel fragments adhering to reactor walls aggregated with freshly synthesized aerogels, generating the observed black agglomerates.

In contrast, ethanol-derived aerogels exhibited enhanced mechanical resilience against fluidic disturbances, enabled by a robust, three-dimensional entangled network of FWCNTs (Figs. 2e and S5d-f). Such entanglement substantially reinforced inter-tube connections, thus preserving morphological integrity even upon contact with reactor walls (Fig. 2b). So, the resultant fibers demonstrated compositional uniformity (Fig. S3b) and reduced mechanical variability (Figs. 2h and S4b).

The mixed acetone-ethanol carbon source approach optimized fiber performance through structural synergy. Straight MWCNT bundles provided a primary oriented framework, and a small number of entangled FWCNTs acted as bridging nodes between bundles, thereby preserving macroscopic alignment and enhancing shear resistance via local mechanical anchoring (Figs. 2f and S5g-i). This integrated “rigid-flexible” structural feature ensured morphological stability and continuous assembly capability under dynamic fluid conditions (Fig. 2c), leading to

compositionally homogeneous fibers (Fig. S3c) with superior strength and minimal mechanical fluctuations (Figs. 2i and S4c).

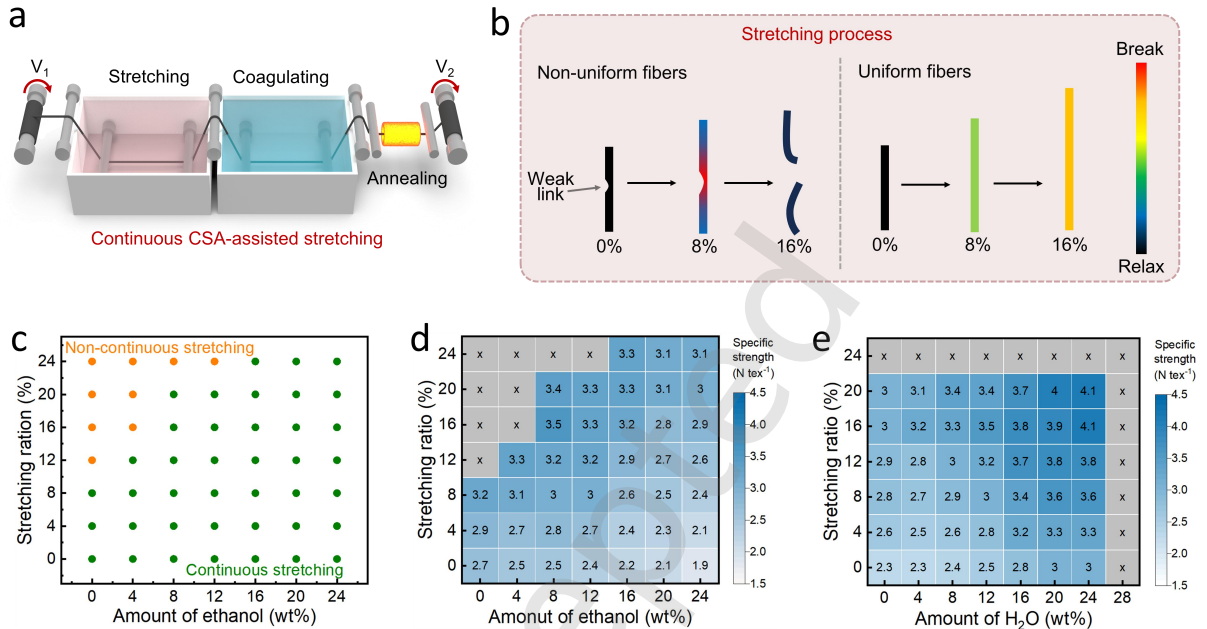


Figure 3 CSA-assisted continuous reinforcement of CNTFs. (a) Schematic illustration of CSA-assisted continuous stretching for CSA-CNTFs fabrication. (b) Force analysis of P-CNTFs under different stretching ratios during CSA-assisted stretching. (c) Effect of ethanol content in the carbon source on the stretchability and stretching ratio of P-CNTFs. Influence of ethanol (d) and water (e) proportions in the carbon source on the specific strength of CSA-CNTFs at different stretching ratios.

Given that the densification and orientation of CNT bundles decisively influenced final fiber performance, we systematically explored the microstructural evolution during CSA-assisted reinforcement of FCCVD-derived P-CNTFs. This process, involving coordinated protonation-induced swelling, orientation-driven stretching, deprotonation-induced contraction and annealing densification (Fig. 3a), critically depended on fiber uniformity, especially during the stretching phase (Fig. 3b). The intrinsic structural heterogeneity of fibers originated from different carbon sources

was further amplified during CSA swelling. As evidenced in Fig. S6, acetone-derived P-CNTFs exhibited non-uniform expansion, whereas ethanol- and mixture-sourced fibers underwent homogeneous swelling, significantly impacting the mechanical response during stretching. Non-uniform fibers contained localized defects that led to stress concentration during stretching, triggering preferential shear-induced slip deformation within structurally compromised regions, thereby prematurely causing local failure and limiting the overall mechanical performance. Conversely, uniform fibers maintained dynamic equilibrium under tensile loading, facilitated by uniform protonation-induced swelling layers that generated consistent frictional resistance gradients between CNT bundles, thereby uniformly distributing stress.

Optimization of fiber uniformity and mechanical performance during CSA-assisted reinforcement relied on synergistic control of carbon-source composition, gradient balancing of water content and dynamic adaptation of stretching procedure, collectively facilitating microstructural reorganization and performance enhancement of P-CNTFs. The ethanol content in the carbon source significantly influenced CNT aerogel assembly behavior and P-CNTFs stretchability in CSA solution (Figs. S7 and 3c). Pure acetone-derived aerogels predominantly comprised highly aligned and straight CNT bundles. Upon increasing ethanol content to 10 wt%, localized entanglement occurred between bundles, evident by spiral or branched bridging structures, substantially enhancing structural stability during fiber formation. Further, increasing ethanol content (≥ 15 wt%) promoted extensive inter-bundle entanglement, exhibiting a clear correlation between ethanol concentration and structural complexity, thus enabling precise tuning of densified fiber microstructures (Fig. S8). At lower ethanol concentrations, continuous and

oriented CNT bundles with minimal inter-bundle gaps dominated the fiber surface morphology. Increasing ethanol content beyond 20 wt% induced evident structural deterioration, characterized by decreased axial orientation, increased bundle curvature and elevated porosity, severely compromising inter-tube load transfer and limiting further mechanical enhancement. Therefore, adjusting ethanol content and stretching conditions enabled fibers synthesized from a carbon source with 8 wt% ethanol to achieve optimal mechanical performance at a stretching ratio of 16% (Fig. 3d and S9).

Notably, higher ethanol concentrations introduced entangled nanotube structures with the reduction of overall mechanical strength, enhanced fiber crystallinity and reduced amorphous carbon content due to the hydroxyl group in ethanol (Fig. S10). To increase crystallinity without inducing additional CNT entanglement, water was introduced into the carbon source as an alternative hydroxyl source. Results demonstrated that increased water content effectively elevated fiber crystallinity without promoting additional nanotube entanglement (Fig. S11), resulting in structurally denser and mechanically superior initial fibers after fiberization (Figs. S12 and S13). Consequently, the optimized structure significantly improved the mechanical performance of fibers after CSA treatment, reaching a remarkable tensile strength of 4.1 N tex^{-1} at a water content of 24 wt% and stretching ratios exceeding 16% (Figs. 3e and S14). Further elevation of water content initiated excessive etching to CNT integrity, significantly reducing crystallinity and linear density of P-CNTFs (Figs. S15-S17), ultimately deteriorating fiber load capacity below the threshold required for effective continuous CSA-assisted stretching treatment.

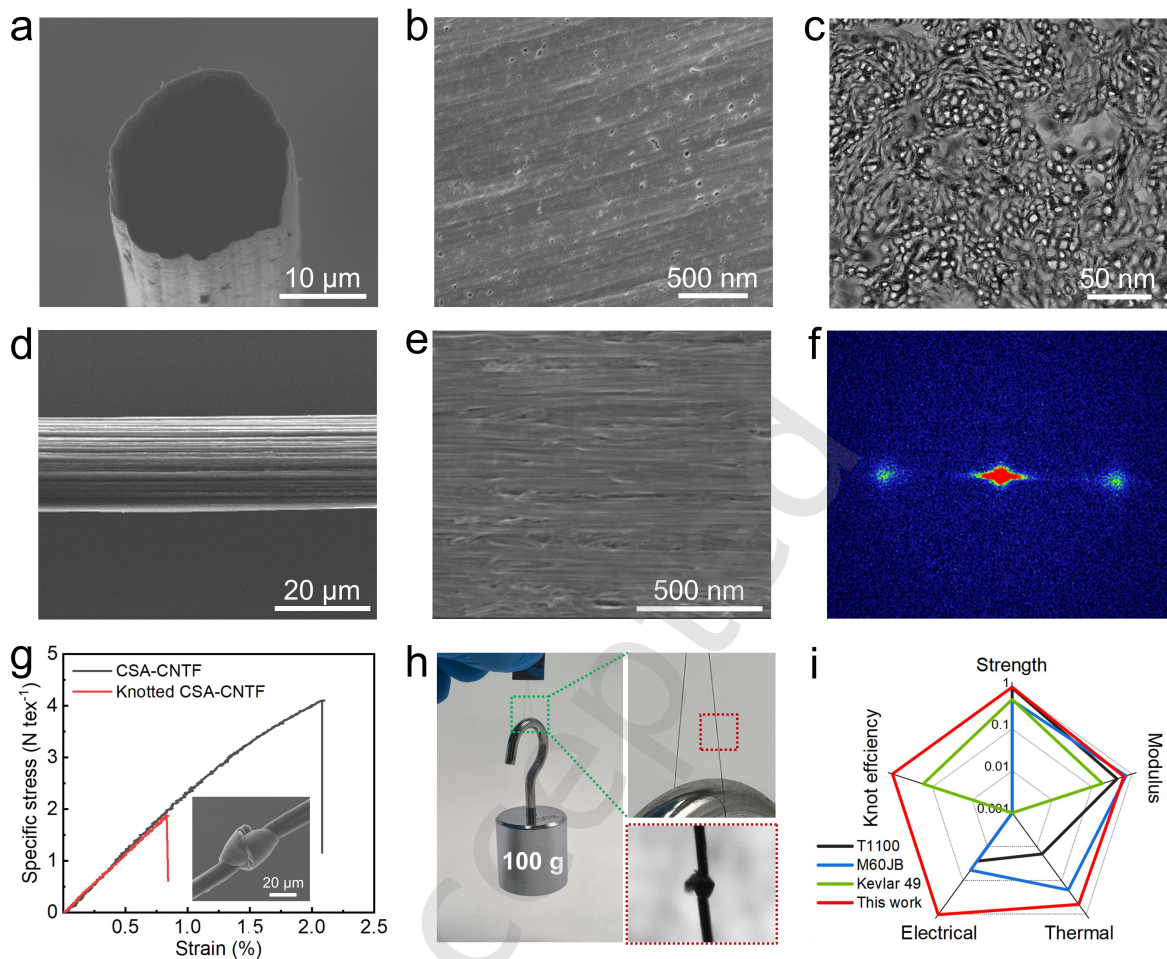


Figure 4 Microstructural characterization and comprehensive performance analysis of CSA-CNTFs. (a) Cross-sectional SEM image and its magnification (b). (c) TEM image. (d) Surface-sectional SEM image and its magnification (e). (f) WAXS pattern. (g) Stress-strain curves. (h) Load-bearing demonstration. (i) Comparative analysis of mechanical, electrical and thermal performance against conventional fibers.

CSA-assisted stretching significantly reshaped the internal CNT bundle microstructure. Fiber diameter was notably reduced from $\sim 25 \mu\text{m}$ to below $20 \mu\text{m}$ (Figs. 4a, S18), effectively eliminating initial layered structures and leaving minimal residual pores below 50 nm (Fig. 4b). TEM characterization revealed solvent-induced

capillary contraction promoted physical densification among nanotube bundles, forming laminated interconnected structures and transforming pore morphology from continuous channels into isolated discrete cavities. This transition effectively shifted the structural dominance from pores to nanotube bundles, establishing a “bundle-encapsulated pore” configuration (Fig. 4c). Crucially, formerly ineffective load-transfer interactions blocked by porous interfaces were markedly improved by post-densification, establishing robust mechanical interlocking and enhanced van der Waals coupling between adjacent CNT bundles, substantially enhancing the load-bearing capacity of CSA-CNTFs. This notable enhancement in densification suggested that a small fraction of entanglements within the P-CNTFs underwent reorientation during the CSA treatment, ultimately resulting in elevated porosity and orientation degree in the CSA-CNTFs.

After CSA processing, CSA-CNTFs underwent pronounced surface reconstruction, featuring characteristic axial wrinkles arising from solvent-evaporation-induced radial contraction and axial stretching-induced topological deformation (Fig. 4d). Additionally, high-resolution SEM image of CSA-CNTFs confirmed the formation of a densely interconnected CNT bundle network interspersed with only isolated nanopores (Fig. 4e). CSA treatment effectively removed interfacial amorphous carbon through a solvent infiltration-recrystallization mechanism, enhancing inter-bundle van der Waals interactions and mechanical interlocking. Consequently, fiber density dramatically increased from 0.82 to 1.45 g cm⁻³, while porosity sharply decreased from 35% to 5%, highlighting profound densification (Fig. S19). Simultaneously, stretching-induced axial reorientation further optimized fiber anisotropy, with the orientation index

improving notably from 0.90 to 0.96 (Figs. 4f and S20).

Mechanical tests utilizing a digital image correlation (DIC)-integrated tensile testing system were conducted to eliminate fiber slippage effects (Fig. S21). The impact of highly oriented and densely-packed configurations in CNTFs on the enhancement of mechanical properties could be directly validated through microscopic analysis of tensile fracture morphology. As depicted in Fig. S22a and b, P-CNTFs displayed hierarchical fracture behavior characterized by extensive bundle pulling-out (100-200 nm in diameter), indicative of weak interfacial cohesion and shear-induced slippage. In contrast, CSA-CNTFs showed drastically reduced fiber pulling-out at fracture surfaces, accompanied by minimal large-diameter bundle remnants (>500 nm). This configuration favored stress transfer through the bundles rather than interfacial slippage, resulting in uniform axial stress distribution and brittle fracture, evidenced by the synchronous axial splitting of bundles (Fig. S22c, d). The poor fracture morphology, combined with the mechanical test data in Fig. S23, further confirms that large CNT bundles can more effectively overcome the limitation of stress non-uniformity in fibers, a theoretical explanation that has been previously reported in the literature. Stress-strain measurements revealed that CSA-CNTFs possessed exceptional specific strength (4.10 N tex^{-1}) and specific modulus (268 N tex^{-1}), exhibiting typical high-modulus characteristics. Furthermore, CSA-CNTFs maintained a remarkable knot strength of 1.89 N tex^{-1} (approximately 45% strength retention), highlighting the combination of high strength and exceptional flexibility (Fig. 4g). Knot-loaded fibers withstood sustained loading of 100 g weight without fracture (Fig. 4h), underscoring structural stability and damage tolerance. Under external load, the densely packed CNT bundles synergistically dispersed local stress

through elastic deformation, effectively preventing brittle failure. This optimized balance of rigidity and flexibility enabled CSA-CNTFs to maintain mechanical integrity under complex deformation. Additionally, continuously produced CSA-CNTFs exhibited synergistic reinforcement of mechanical, electrical and thermal performance (Fig. S23). An axial thermal conductivity reaching $400 \text{ W m}^{-1} \text{ K}^{-1}$ resulted from continuous and highly aligned CNT bundles that minimized interfacial phonon scattering. Additionally, fibers demonstrated a specific electrical conductivity up to $1480 \text{ S m}^2 \text{ kg}^{-1}$ in vacuum, with a current-carrying capacity exceeding 45000 A cm^{-2} , attributed to tight π - π stacking between CNT interfaces and reduced defects. A comparative analysis of CSA-CNTFs and commercial state-of-the-art fibers, based on normalized properties, revealed that CSA-CNTFs achieved a groundbreaking equilibrium between mechanical robustness and functional performance (Fig. 4i).

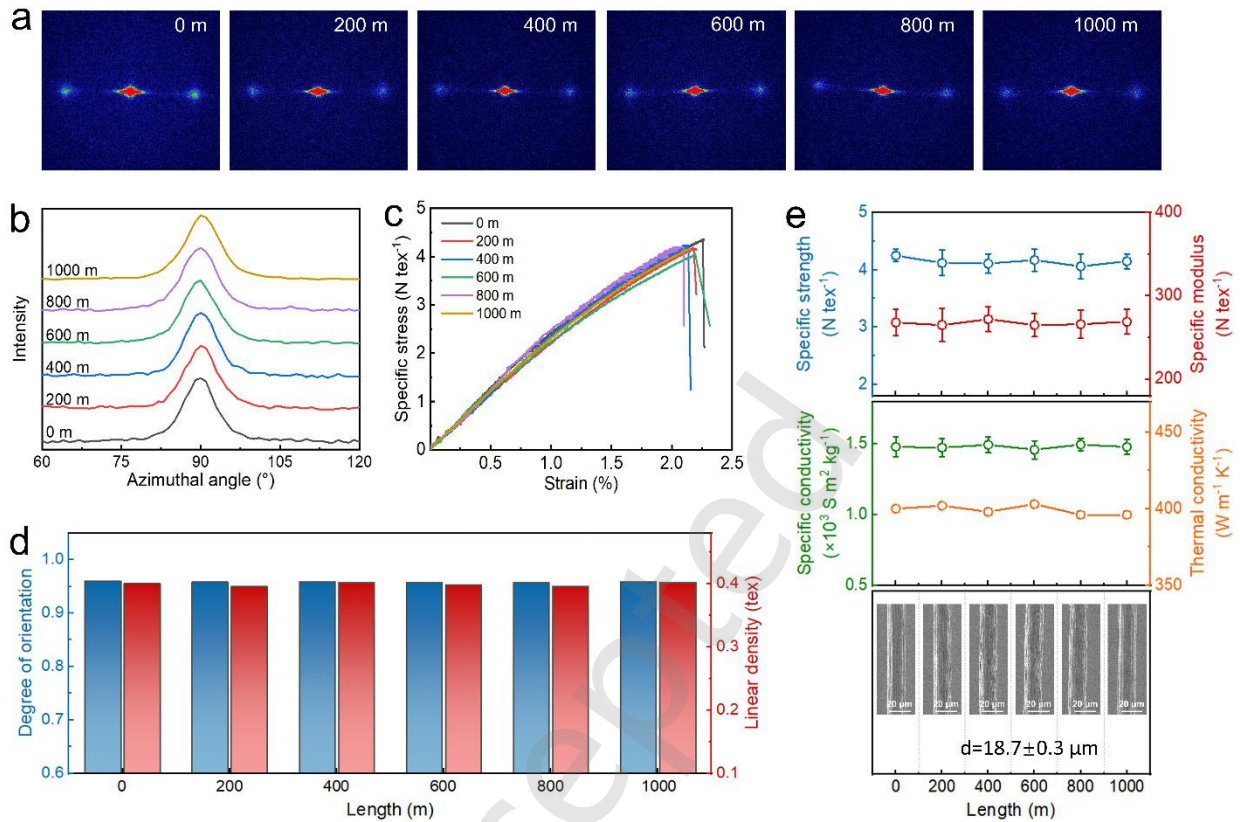


Figure 5 Microstructure and performance analysis of scalable CSA-CNTFs at different axial positions. (a) WAXS patterns. (b) Azimuthal intensity profiles. (c) Stress-strain curves. (d) Orientation degree and linear density. (e) Comprehensive evaluation of mechanical, electrical, thermal and structural properties.

Continuous kilometer-scale CSA-CNTFs were successfully fabricated using a custom-built processing platform (Fig. S24). Structural and performance uniformity were systematically evaluated through multi-point characterization at 200 m intervals. WAXS characterization revealed remarkable consistency in diffraction peak intensity, position and symmetry across different axial locations, providing initial evidence of uniform spatial orientation within the fibers (Fig. 5a). Quantitative orientation analysis was performed by examining WAXS azimuthal intensity profiles. As envisioned in Figs. 5b, d, the variation in FWHM across all sampling points was

below 0.2° , and a uniform orientation index of 0.96 was available, further substantiating excellent macroscopic alignment homogeneity. Complementary SAXS and cross-sectional electron microscopy collectively revealed homogeneous structural characteristics spanning from nanoscale to microscale dimensions, thus presenting comprehensive evidence of structural uniformity at multiscale levels (Figs. S26 and S27). These analyses underlined that the synergistic effects arising from multilevel structural ordering fundamentally accounted for the superior consistency in macroscopic fiber performance.

The kilometer-scale continuous CSA-CNTFs also exhibited exceptional uniformity in diameter, with no discernible changes observed in the microscopic surface morphology of fibers (Fig. 5e). Optimization of processing parameters yielded highly reproducible axial stress-strain behavior, characterized by near-identical specific strength, modulus, and elongation at break across different fiber segments [33] (Fig. 5c). Statistical evaluations revealed relative deviations in specific strength and modulus with less than 7% and 10%, respectively, among ten tested samples from identical fiber positions, underscoring outstanding uniformity. Moreover, variations in specific strength and modulus along the fiber axis remained below 3% and 5%, respectively, demonstrating exceptional long-range consistency. Electrical and thermal measurements corroborated mechanical uniformity, with fluctuations below 5% along the fiber length (Fig. 5e). Such strong correlations between processing, structural alignment and fiber performance confirmed that precise control over nanotube bundle orientation and interfacial interactions enabled uniform intrinsic properties across multiple length scales, thus laying a foundational basis for industrial-scale applications.

4. Conclusions

In summary, this work proposed a mixed carbon-source strategy that precisely tailored CNT aerogels with optimal alignment and moderate entanglement, ensuring intrinsic structural uniformity and enabling subsequent densification into densely packed architectures under CSA-assisted stretching, ultimately yielding kilometer-scale high-performance CNTFs. Impressively, CSA-CNTFs boasted superior tensile strength (4.10 ± 0.17 N tex⁻¹), modulus (268 ± 16 N tex⁻¹), electrical conductivity (1480 S m² kg⁻¹) and thermal conductivity (400 W m⁻¹ K⁻¹), combined with outstanding flexibility indicated by high knot-strength retention (>45%). Comprehensive multi-point characterization validated exceptional structural and property uniformity across kilometer-scale lengths. These findings underscored the critical importance of precisely controlling nanotube alignment and interfacial interactions, providing a significant technological foundation and viable pathway toward large-scale practical applications of advanced high-performance CNTFs. In contrast with the randomly distributed CNTs in the polymer matrix [34], the CNTFs with oriented structures will enhance the mechanical properties, increase the electrical conductivity and thermal conductivity [35] of the produced nanocomposites.

Acknowledgments

Yutao Niu, Zhao He and Shan Wang contributed equally to this work. The authors are grateful to the financial support from the National Key Research and Development Program of China (2022YFA1203304), the National Natural Science Foundation of China (52272081, 52162007, 52163032), the Jiangxi Provincial Key Laboratory of

Carbonene Materials (No. 2024SSY05101), Jiangxi Province Talent Team Plan (20243BCE51008). We also extend our gratitude to Nano-X from the Suzhou Institute of Nano-Tech and Nano-Bionics (SINANO), Chinese Academy of Sciences, for providing technical support for the WAXS characterization.

Declaration of competing interest

The authors declare no conflict of interest.

Data availability

The datasets generated and analyzed during the current study are available from the corresponding author upon reasonable request.

Appendix A. Supplementary data

Supplementary data to this article can be found in the online version.

REFERENCES

- [1] Mu, J. K.; Jung de Andrade, M.; Fang, S. L.; Wang, X. M.; Gao, E. L.; Li, N.; Kim, S. H.; Wang, H. Z.; Hou, C. Y.; Zhang, Q. H. et al. Sheath-run artificial muscles. *Science* **2019**, *365*, 150-155.
- [2] Kinloch, I. A.; Suhr, J.; Lou, J.; Young, R. J.; Ajayan, P. M. Composites with carbon nanotubes and graphene: an outlook. *Science* **2018**, *362*, 547-553.
- [3] Behabtu, N.; Young, C. C.; Tsentalovich, D. E.; Kleinerman, O.; Wang, X.; Ma, A. W. K.; Bengio, E. A.; ter Waarbeek, R. F.; de Jong, J. J.; Hoogerwerf, R. E. et al. Strong, light, multifunctional fibers of carbon nanotubes with ultrahigh conductivity. *Science* **2013**, *339*, 182-186.
- [4] Zhang, X. H.; Lu, W. B.; Zhou, G. H.; Li, Q. W. Understanding the mechanical and conductive properties of carbon nanotube fibers for smart electronics. *Adv. Mater.* **2019**, *32*, 1902028.
- [5] Bai, Y. X.; Zhang, R. F.; Ye, X.; Zhu, Z. X.; Xie, H. H.; Shen, B. Y.; Cai, D. L.; Liu, B. F.; Zhang, C. X.; Jia, Z. et al. Carbon nanotube bundles with tensile strength over 80 GPa. *Nat. Nanotech.* **2018**, *13*, 589-595.

- [6] Yue, H. J.; Xing, H. Z.; Qin, L. X.; Bai, Y. X.; Li, X. Y.; Wei, F. Double - walled carbon nanotubes with dynamic strength of over 90 GPa enhanced by intershell friction. *Adv. Mater.* **2025**, *337*, 2414643.
- [7] Koziol, K.; Vilatela, J.; Moisala, A.; Motta, M.; Cunniff, P.; Sennett, M.; Windle, A. High-performance carbon nanotube fiber. *Science* **2007**, *318*, 1892-1895.
- [8] Huang, J. K.; Guo, Y. Z.; Lei, X. D.; Chen, B.; Hao, H.; Luo, J. J.; Sun, T. Z.; Jian, M. Q.; Gao, E. L.; Wu, X. Q. et al. Fabricating ultrastrong carbon nanotube fibers via a microwave welding interface. *ACS Nano* **2024**, *18*, 14377-14387.
- [9] Yang, Z. C.; Yang, Y. N.; Huang, Y. F.; Shao, Y. Y.; Hao, H.; Yao, S. D.; Xi, Q. Q.; Guo, Y. B.; Tong, L. M.; Jian, M. Q. et al. Wet-spinning of carbon nanotube fibers: dispersion, processing and properties. *Natl. Sci. Rev.* **2024**, *11*. nwae203.
- [10] Cho, Y. S.; Lee, J. W.; Jung, Y.; Park, J. Y.; Park, J. S.; Kim, S. M.; Yang, S. J.; Park, C. R. Super-toughness carbon nanotube yarns by bio-inspired nano-coiling engineering. *Adv. Sci.* **2024**, *11*. 2400460.
- [11] Hu, Z. C.; Sun, X. C.; Zhang, X. S.; Jia, X. Z.; Feng, X. T.; Cui, M. W.; Gao, E. L.; Qian, L.; Gao, X.; Zhang, J. Kinetic modulation of carbon nanotube growth in direct spinning for high-strength carbon nanotube fibers. *J. Am. Chem. Soc.* **2024**, *146*, 11432-11439.
- [12] Vilatela, J. J.; Elliott, J. A.; Windle, A. H. A model for the strength of yarn-like carbon nanotube fibers. *ACS Nano* **2011**, *5*, 1921-1927.
- [13] Gao, E. L.; Lu, W. B.; Xu, Z. P. Strength loss of carbon nanotube fibers explained in a three-level hierarchical model. *Carbon* **2018**, *138*, 134-142.
- [14] Shi, H. L.; Shi, Q. Q.; Zhan, H.; Ai, J. J.; Chen, Y. T.; Wang, J. N. High-strength carbon nanotube fibers from purity control by atomized catalytic pyrolysis and alignment improvement by continuous large prestraining. *Nano Lett.* **2023**, *23*, 10739-10747.
- [15] Ryu, K.-H.; Kim, J.-G.; Lee, D.; Kim, S. G.; Ku, B.-C.; Hwang, J. Y.; Jeong, K.-U.; Kim, N. D.; Kim, D.-Y. Boost up the mechanical and electrical property of CNT fibers by governing lyotropic liquid crystalline mesophases with aramid polymers for robust lightweight wiring applications. *Adv. Fiber Mater.* **2022**, *5*, 514-526.
- [16] Lee, D.; Kim, S. G.; Hong, S.; Madrona, C.; Oh, Y.; Park, M.; Komatsu, N.; Taylor, L. W.; Chung, B.; Kim, J. Ultrahigh strength, modulus, and conductivity of graphitic fibers by macromolecular coalescence. *Sci. Adv.* **2022**, *8*, eabn0939.
- [17] Liu, F. Y.; Wang, Q. Q.; Zhai, G. X.; Xiang, H. X.; Zhou, J. L.; Jia, C.; Zhu, L. P.; Wu, Q. L.; Zhu, M. F. Continuously processing waste lignin into high-value carbon

- nanotube fibers. *Nat. Commun.* **2022**, *13*, 5755.
- [18] Wu, K. J.; Zhang, Y. Y.; Yong, Z. Z.; Li, Q. W. Continuous preparation and performance enhancement techniques of carbon nanotube fibers. *Acta Phys. -Chim. Sin.* **2021**, *38*, 2106034.
- [19] Cho, Y. S.; Park, J. Y.; Lee, J. W.; Kim, J. S.; Kim, H. W.; Park, Y. J.; Yang, S. J.; Park, C. R. Effects of multidimensional-assembly-structures of CNTs on the evolution of various properties of resultant products therefrom. *Mater. Chem. Phys.* **2024**, *322*, 129528.
- [20] Fernández-Toribio, J. C.; Alemán, B.; Ridruejo, Á.; Vilatela, J. J. Tensile properties of carbon nanotube fibres described by the fibrillar crystallite model. *Carbon* **2018**, *133*, 44-52.
- [21] Zhang, X. H.; Li, Q. W. Enhancement of friction between carbon nanotubes: an efficient strategy to strengthen fibers. *ACS Nano* **2010**, *4*, 312-316.
- [22] Wu, K. J.; Wang, B.; Niu, Y. T.; Wang, W. J.; Wu, C.; Zhou, T.; Chen, L.; Zhan, X. H.; Wan, Z. Y; Wang, S. et al. Carbon nanotube fibers with excellent mechanical and electrical properties by structural realigning and densification. *Nano Res.* **2023**, *16*, 12762-12771.
- [23] Rahimian-Koloor, S.M.; Shokrieh, M.M. Investigating the effect of the curing-induced residual stress on the mechanical behavior of carbon nanotube/epoxy nanocomposites by molecular dynamics simulation. *Eng. Sci.* **2023**, *22*, 817.
- [24] Han, Z. Y.; Niu, Y. T.; Shi, X. T.; Pan, D.; Liu, H.; Qiu, H.; Chen, W. H.; Xu, B. B.; El-Bahy, Z. M.; Hou, H. et al. MXene@ c-MWCNT adhesive silica nanofiber membranes enhancing electromagnetic interference shielding and thermal insulation performance in extreme environments. *Nano-Micro Lett.* **2024**, *16*, 195.
- [25] Zhang, X. S.; Lei, X. D.; Jia, X. Z.; Sun, T. Z.; Luo, J. J.; Xu, S. C.; Li, L. J.; Yan, D.; Shao, Y. L.; Yong, Z. Z. et al. Carbon nanotube fibers with dynamic strength up to 14 GPa. *Science* **2024**, *384*, 1318-1323.
- [26] Wang, J. N.; Luo, X. G.; Wu, T.; Chen, Y. High-strength carbon nanotube fibre-like ribbon with high ductility and high electrical conductivity. *Nat. Commun.* **2014**, *5*, 3848.
- [27] Park, J. S.; Park, J. Y.; Kim, J. S.; Kang, Y.; Kim, S. M.; Song, K. S.; Kim, H. W.; Park, Y. J.; Kim, G.; Song, K. et al. Molecular-level network engineering of crosslinker towards high-performance carbon nanotube fiber. *Compos. Part B-Eng.* **2024**, *275*, 111338.
- [28] Li, L. J.; Sun, T. Z.; Lu, S. C.; Chen, Z.; Xu, S. C; Jian, M. Q.; Zhang, J. Graphene

- interlocking carbon nanotubes for high-strength and high-conductivity fibers. *ACS Appl. Mater. Interfaces* **2023**, *15*, 5701-5708.
- [29] Lee, J.; Lee, D.-M.; Jung, Y.; Park, J.; Lee, H. S.; Kim, Y.-K.; Park, C. R.; Jeong, H. S.; Kim, S. M. Direct spinning and densification method for high-performance carbon nanotube fibers. *Nat. Commun.* **2019**, *10*, 2962.
- [30] Zhang, X.; Volder, M. D.; Zhou, W. B.; Issman, L.; Wei, X. J.; Kaniyoor, A.; Portas, J. T.; Smail, F.; Wang, Z. B.; Wang, Y. C. et al. Simultaneously enhanced tenacity, rupture work, and thermal conductivity of carbon nanotube fibers by raising effective tube portion. *Science Advances* **2022**, *8*, eabq3515.
- [31] Niu, Y. T.; He, Z.; Wang, S.; Yang, Z. P.; Ayob, E. A.; Amin, M. A.; Zhao, L. M.; Cao, Y. F.; Guo, Z. H.; Zhang, Y. Y. Directed assembly and microstructural control of carbon nanotube fibers via carbon source manipulation. *ACS Appl. Nano Mater.* **2025**, *8*, 5730-5738.
- [32] Zhu, J. H.; Cheng, L.; Zhang, S. Y.; Lan, D.; Wu, G. R.; Gao, Z. G.; Jia, Z. R. 0D/1D hollow heterogeneous structure to induce self-assembly of CNTs for optimized self-anticorrosion and electromagnetic wave absorption performance. *Carbon* **2025**, *238*, 120310.
- [33] Zhu, Z.; Zhang, H.; Ma, Y.; Yang, Z.; Chen, Z.; Zhang, H. Preparing high-quality monolithic carbon nanotubes reinforced silica aerogel composites based on a vacuum freeze-drying method. *Eng. Sci.* **2024**, *31*, 1149
- [34] Zhu, J.; Cheng, L.; Zhang, S.; Lan, D.; Wu, G.; Gao, Z.; Jia, Z. 0D/1D Hollow heterogeneous structure to induce self-assembly of CNTs for optimized self-anticorrosion and electromagnetic wave absorption performance. *Carbon*, **2025**, *238*, 120310.
- [35] Wang, C.; Zhang, Z.; Xu, X.; Wu, H.; Liu, D.; Xie, P.; Liu, C. Flexible and biocompatible polystyrene/multi-walled carbon nanotubes films with high permittivity and low loss. *ES Mater. Manuf.* **2023**, *19*, 791.

Electronic Supplementary Material

**Continuous carbon nanotube fiber with an extremely high average
specific strength of 4.1 N/tex**

Yutao Niu^{1,2,3,\$}, Zhao He^{3,4,\$}, Shan Wang^{3,5,\$}, Yichi Zhang^{1,2,3}, Zhengpeng Yang⁵, Yongyi Zhang^{1,2,3,*}, Zhenzhong Yong^{1,2,3}, Kunjie Wu^{2,3}, Liming Zhao^{2,*}, Zhanhu Guo^{6,*}, Muqiang Jian^{7,*}, and Qingwen Li^{1,2,*}

¹ School of Nano-Tech and Nano-Bionics, University of Science and Technology of China, Hefei 230026, China

² Key Laboratory of Multifunctional Nanomaterials and Smart Systems, Suzhou Institute of Nano-Tech and Nano-Bionics, Chinese Academy of Sciences, Suzhou 215123, China

³ Division of Nanomaterials and Jiangxi Key Lab of Carbonene Materials, Jiangxi Institute of Nanotechnology, Nanchang 330200, China

⁴ College of Chemistry and Chemical Engineering/Film Energy Chemistry for Jiangxi Provincial Key Laboratory (FEC), Nanchang University, 999 Xuefu Avenue, Nanchang 330031, China

⁵ Henan Key Laboratory of Materials on Deep-Earth Engineering, School of Materials Science and Engineering, Henan Polytechnic University, Jiaozuo 454003, China

⁶ Integrated Composites Lab, Department of Mechanical and Construction Engineering, Northumbria University, Newcastle Upon Tyne NE1 8ST, UK

⁷ Beijing Graphene Institute (BGI), Beijing 100095, China

✉ Address correspondence to Yongyi Zhang, yyzhang2011@sinano.ac.cn; Liming Zhao, lmzhao2019@sinano.ac.cn; Zhanhu Guo, zhanhu.guo@northumbria.ac.uk; Muqiang Jian, jianmqcnc@pku.edu.cn; Qingwen Li, qwli2007@sinano.ac.cn

Supporting information to <https://doi.org/10.26599/NR.2025.94907584>

Supplementary Figures

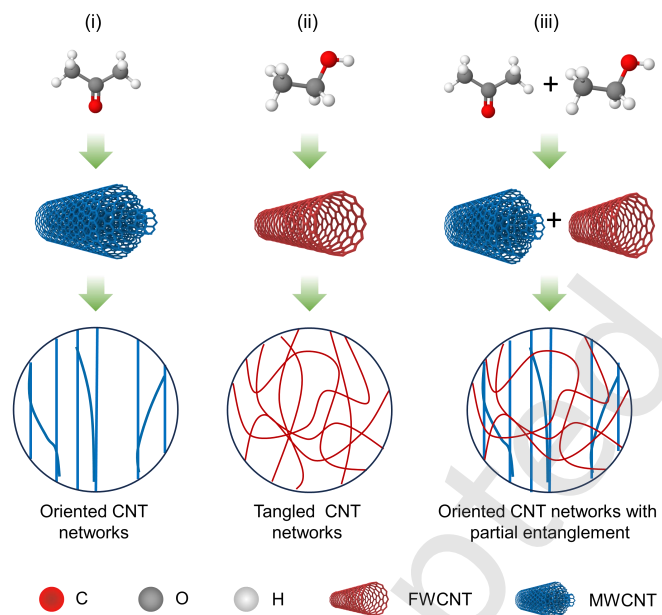


Figure S1. Structural variations and assembled aerogel networks of CNTs grown from different carbon sources.

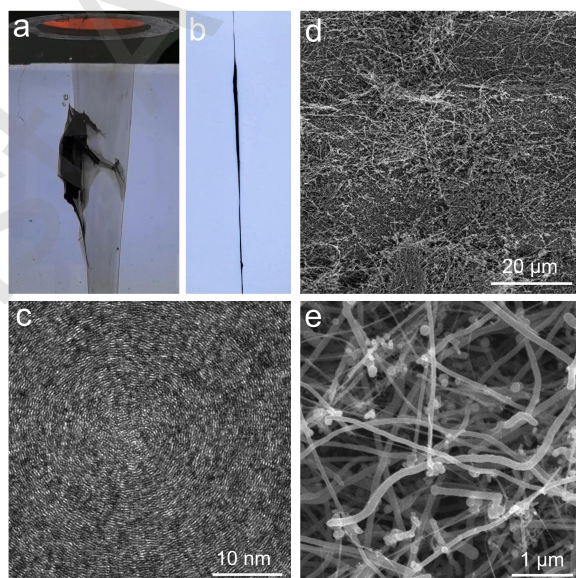


Figure S2. Photographs of aerogel agglomeration (a) and densification (b) during FCCVD. TEM image (c) and SEM images (d,e) of aerogel agglomerates.

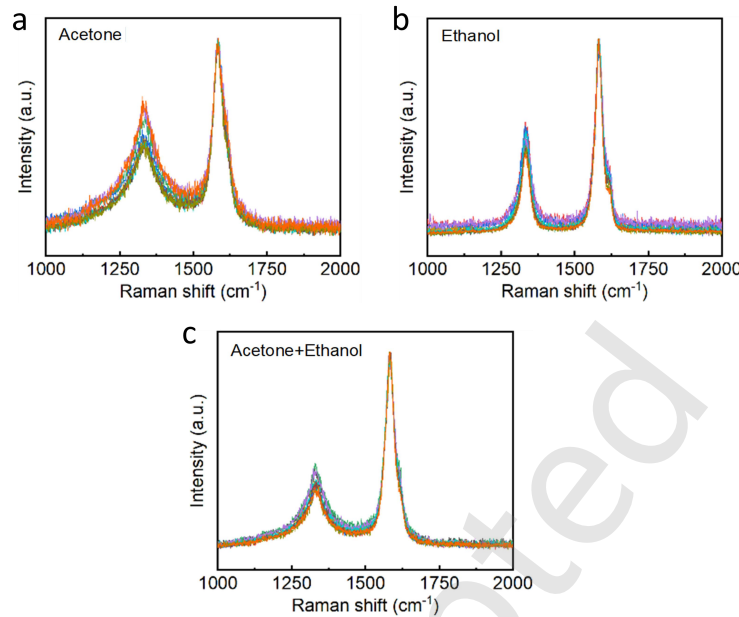


Figure S3. Raman analyses of P-CNTFs derived from different carbon sources.

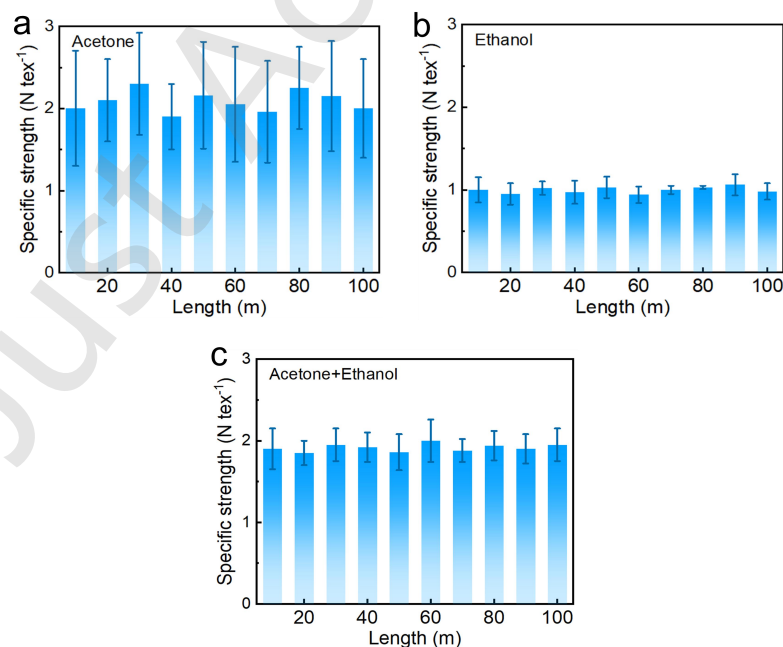


Figure S4. Specific strength analyses of P-CNTFs derived from different carbon sources.

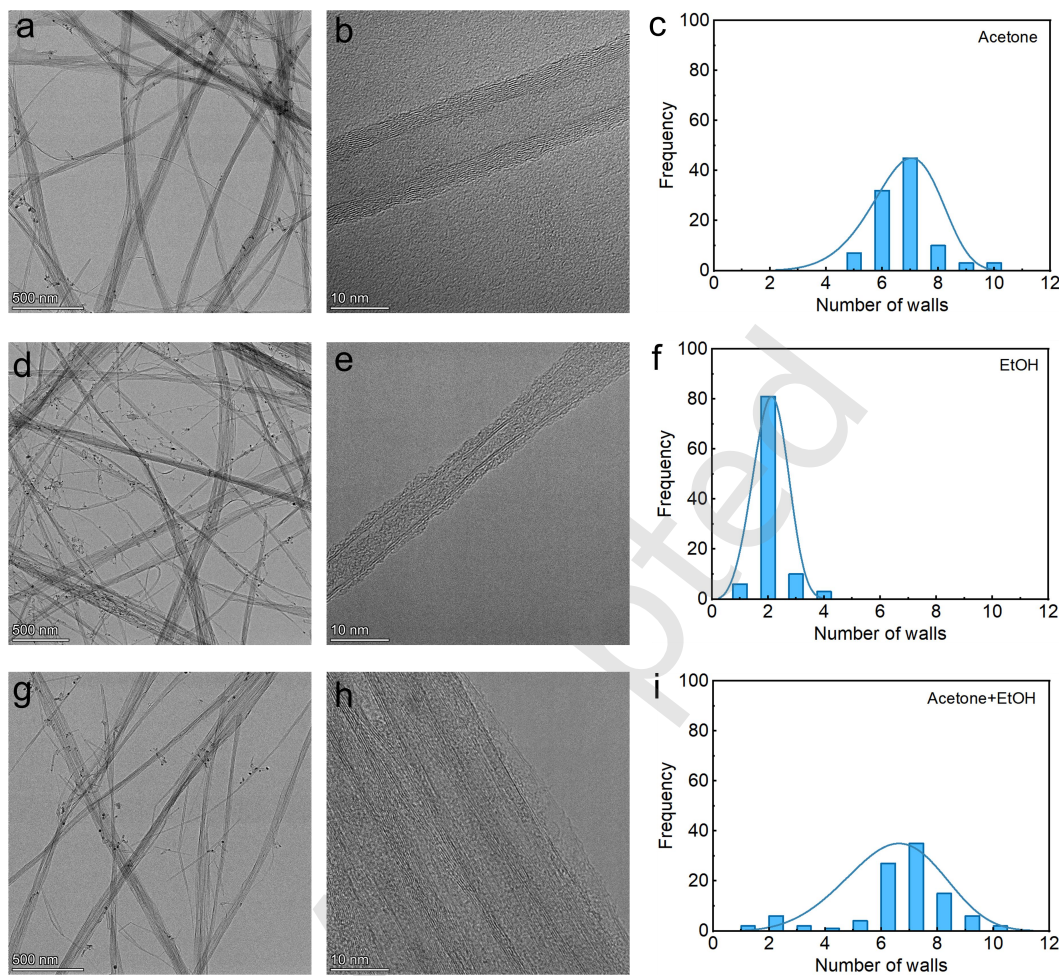


Figure S5. TEM images and wall-number distributions of CNTFs derived from acetone (a-c), ethanol (d-f) and acetone-ethanol (g-i) carbon sources.

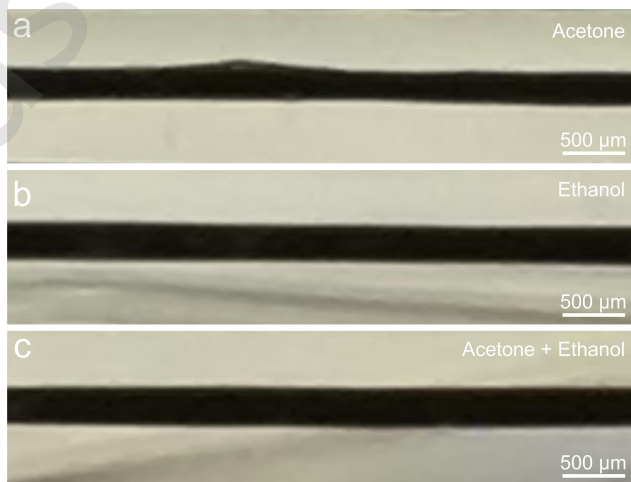


Figure S6. Photographs of P-CNTFs derived from acetone (a), ethanol (b) and acetone-ethanol

(c) carbon sources during CSA treatment.

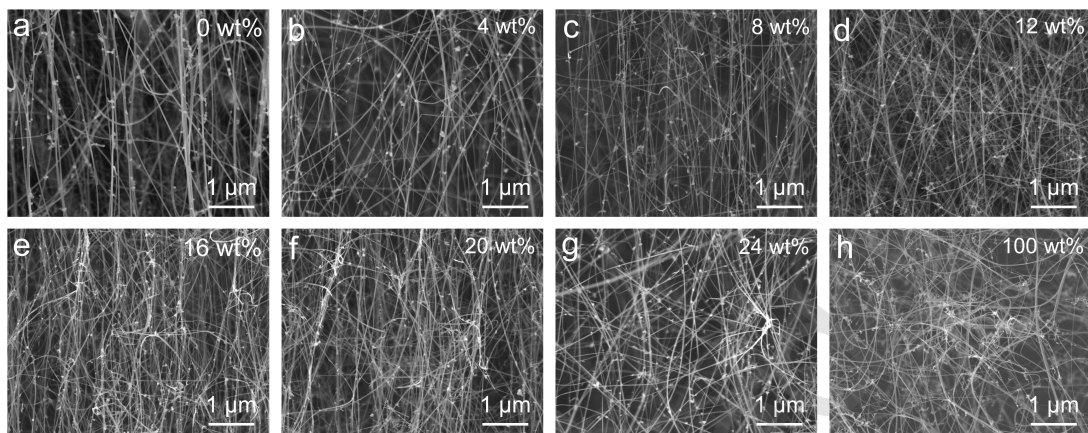


Figure S7. SEM images of CNT aerogels fabricated by acetone-ethanol carbon sources with different ethanol contents.

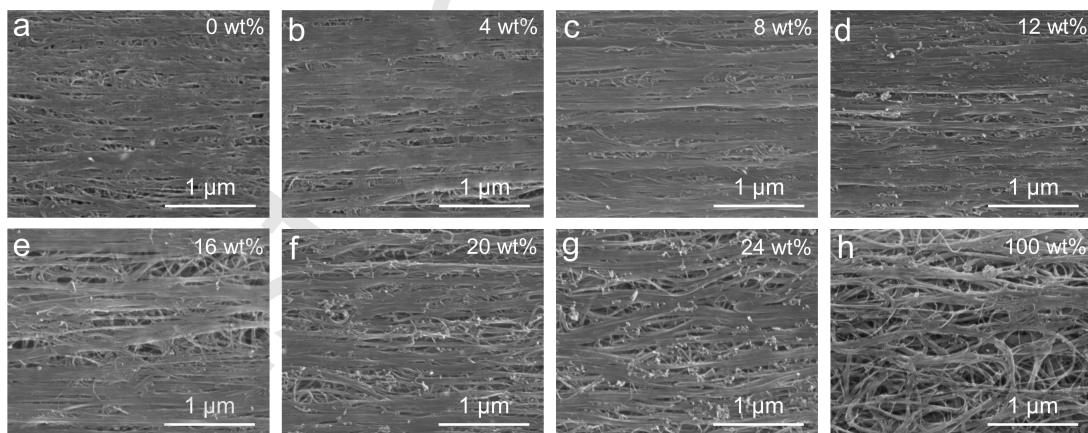


Figure S8. SEM images of P-CNTFs fabricated by acetone-ethanol carbon sources with different ethanol contents.

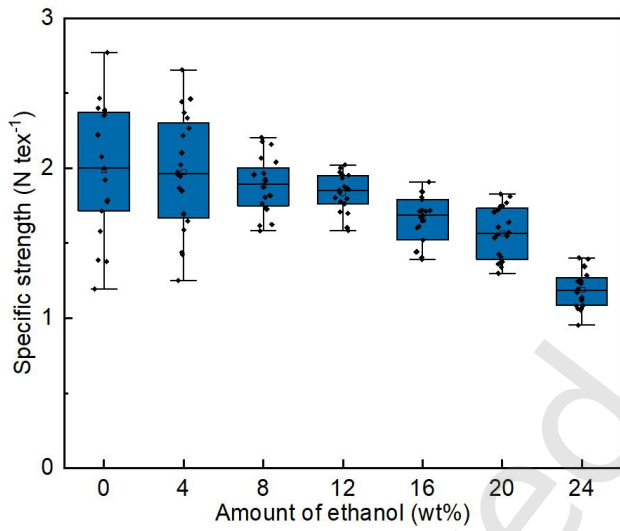


Figure S9. Specific strength uniformity analysis of P-CNTFs fabricated by acetone-ethanol carbon sources with different ethanol contents.

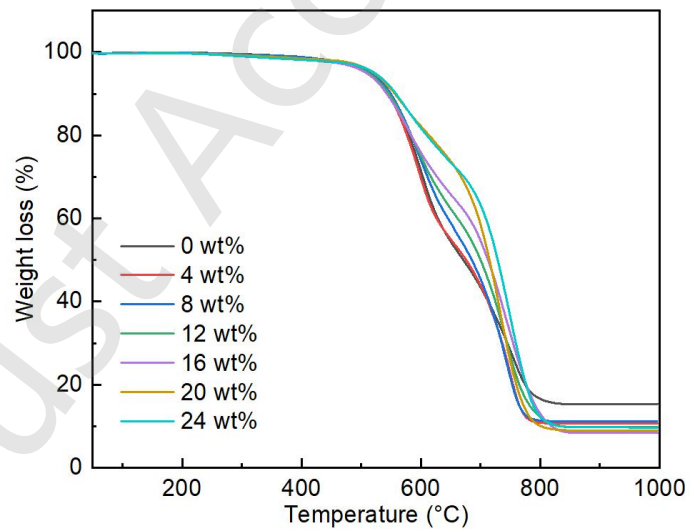


Figure S10. TG curves of P-CNTFs fabricated by acetone-ethanol carbon sources with different ethanol contents.

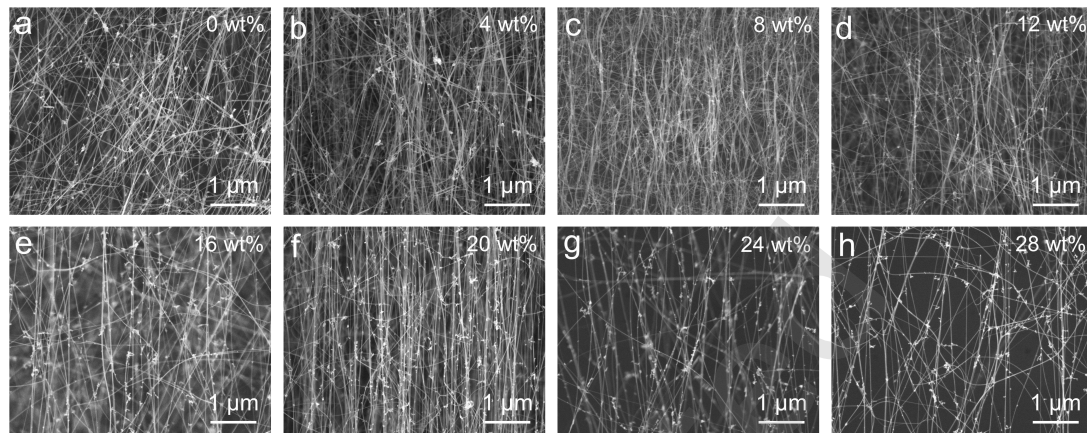


Figure S11. SEM images of CNT aerogels fabricated by acetone-ethanol carbon sources with different water contents.

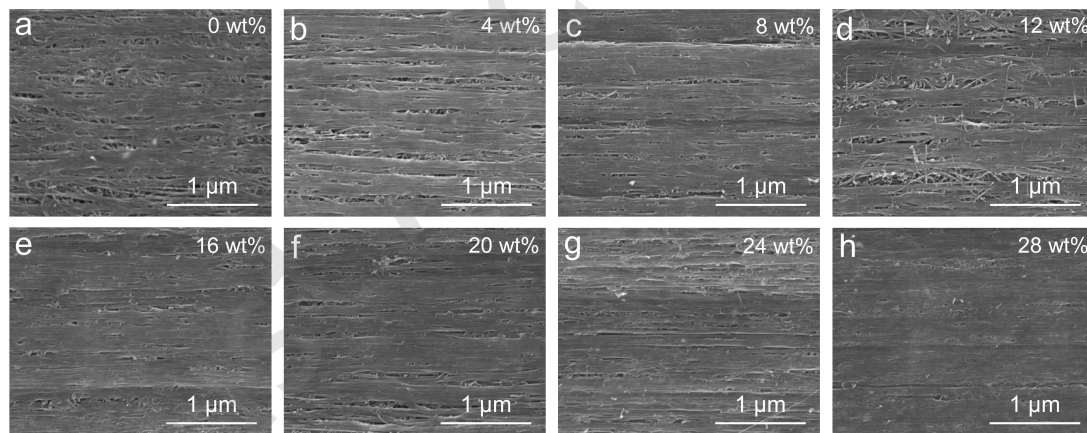


Figure S12. SEM images of P-CNTFs fabricated by acetone-ethanol carbon sources with different water contents.

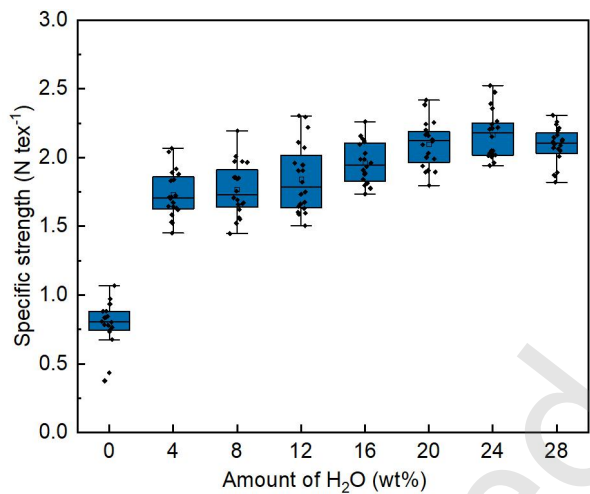


Figure S13. Specific strength uniformity analysis of P-CNTFs fabricated by acetone-ethanol carbon sources with different water contents.

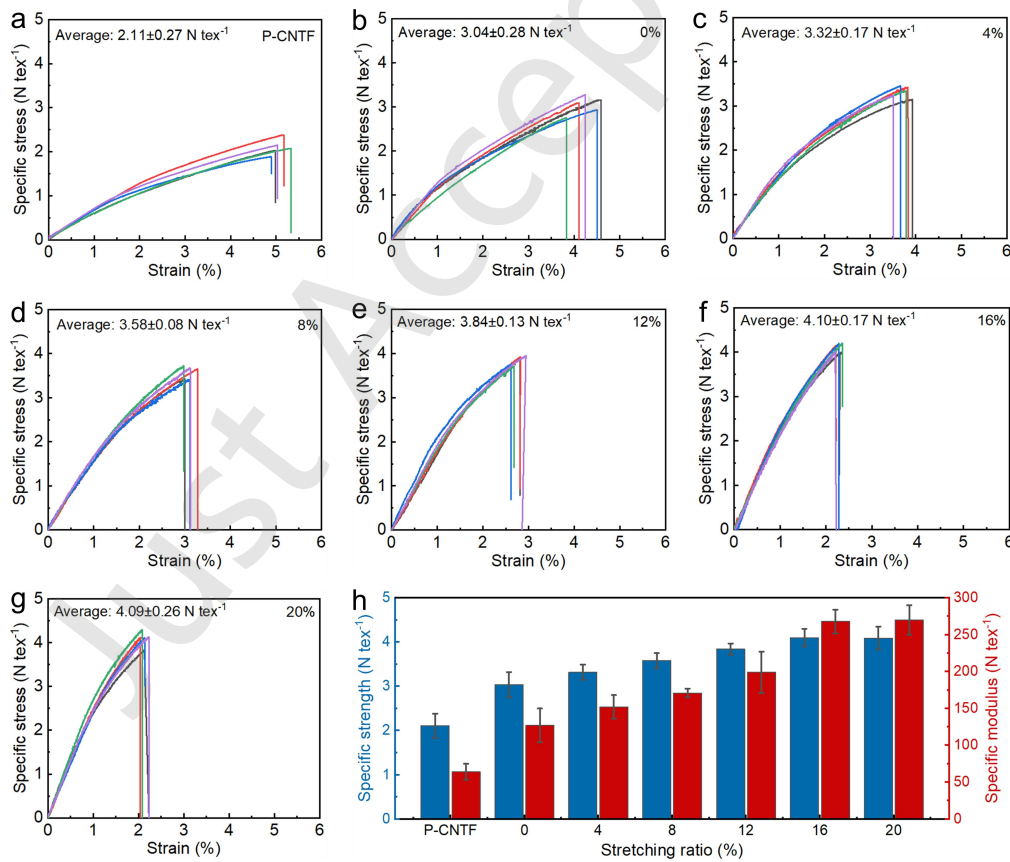


Figure S14. Stress-strain curves of P-CNTFs (a) and CSA-CNTFs with different stretching ratios in CSA (b-g). (h) Specific strength and modulus of P-CNTFs and CSA-CNTFs with different stretching ratios.

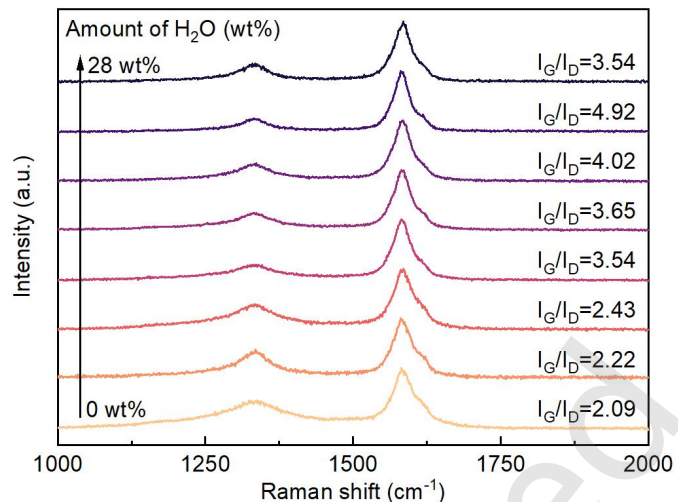


Figure S15. Raman analyses of P-CNTFs fabricated by acetone-ethanol carbon sources with different water contents.

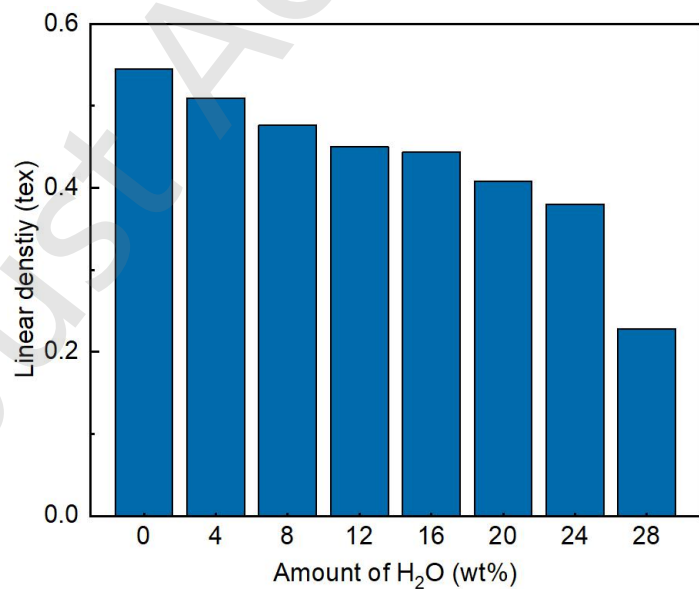


Figure S16. Linear density of P-CNTFs fabricated by acetone-ethanol carbon sources with different water contents.

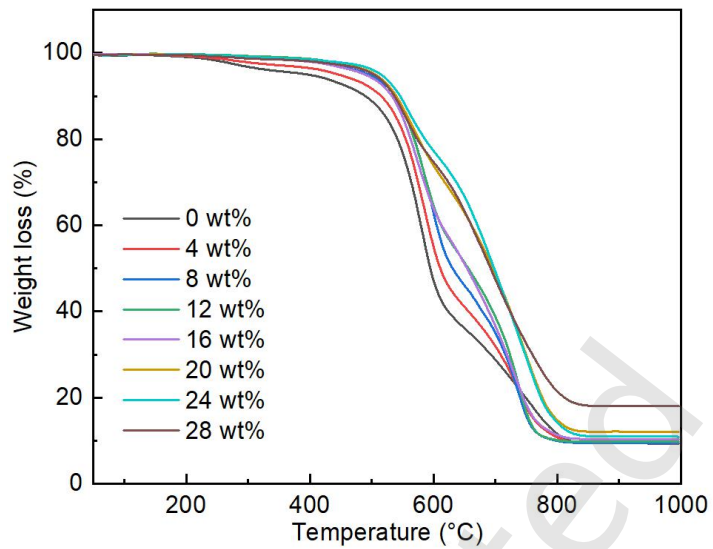


Figure S17. TG curves of P-CNTFs fabricated by acetone-ethanol carbon sources with different water contents.

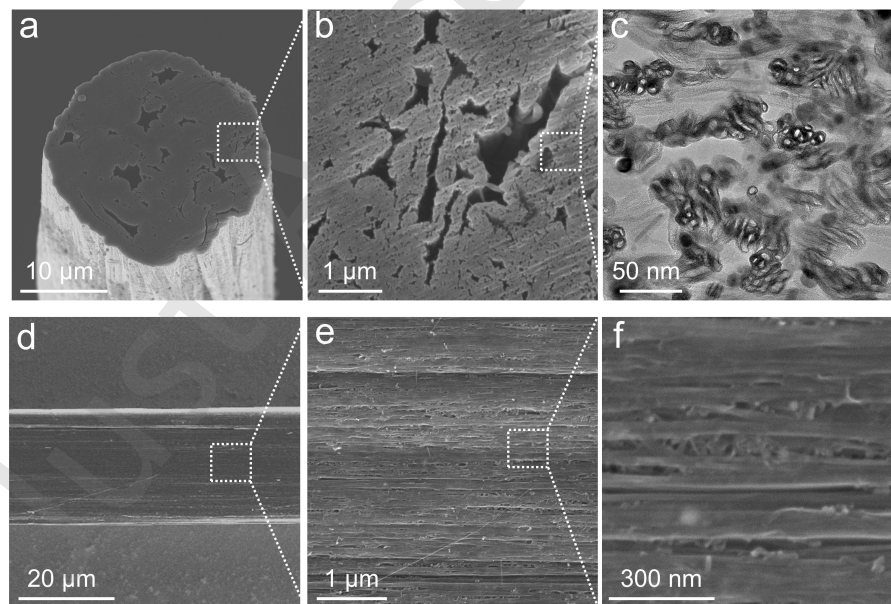


Figure S18. Cross-sectional SEM images (a,b) and TEM image (c) of P-CNTF. (d-e) Surface-sectional SEM images of P-CNTF.

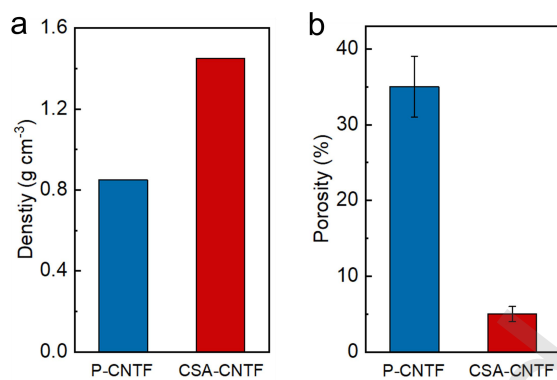


Figure S19. Density (a) and porosity (b) of P-CNTF and CSA-CNTF.

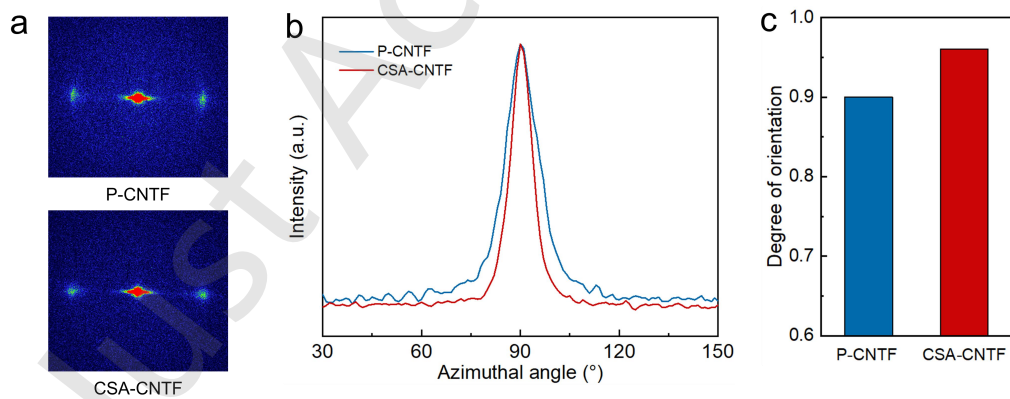


Figure S20. WAXS patterns (a), azimuthal intensity profiles (b) and orientation degree (c) of P-CNTF and CSA-CNTF.

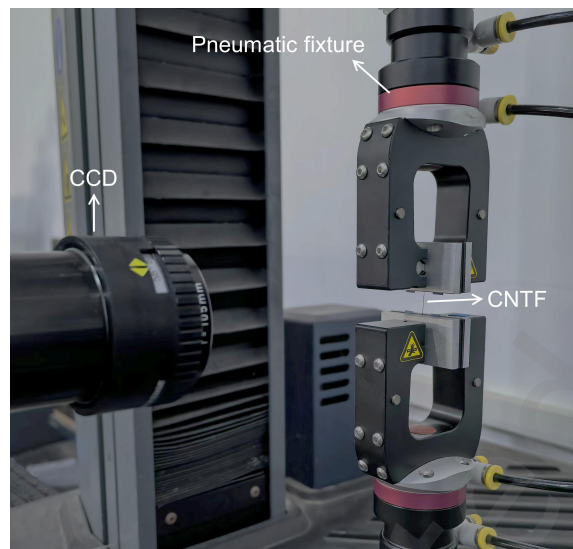


Figure S21. Photograph of DIC-integrated universal mechanical testing system.

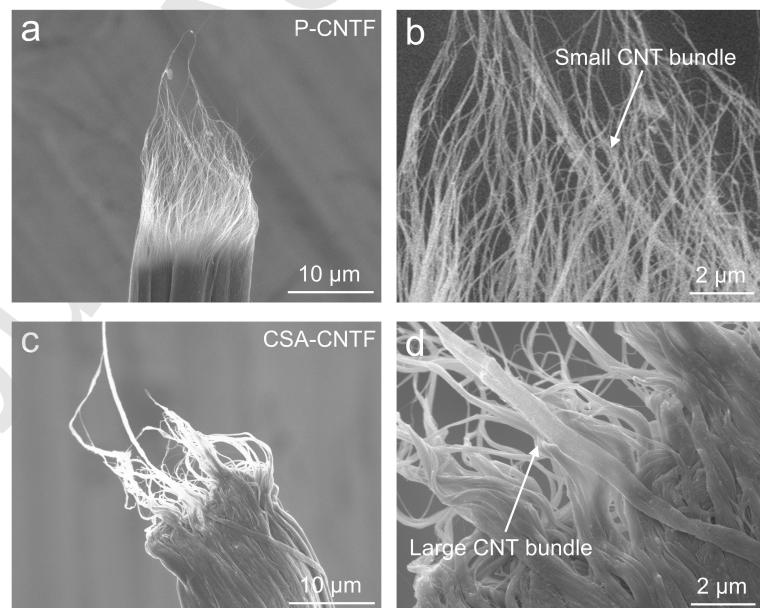


Figure S22. SEM images of P-CNTF (a,b) and CSA-CNTF (c,d) after tensile failure.

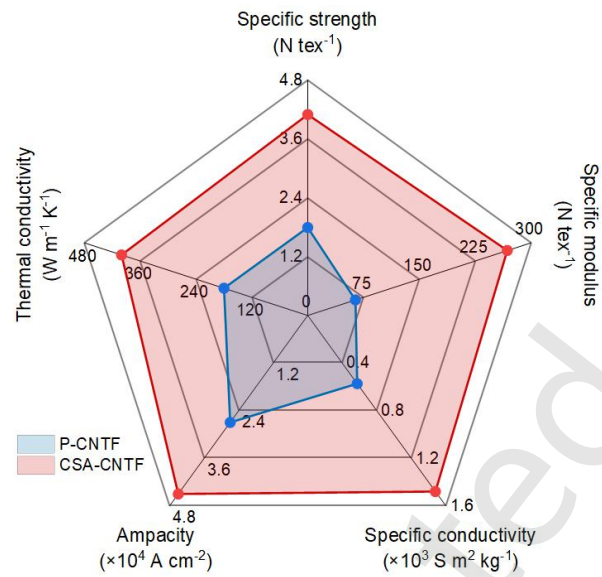


Figure S23. Comparative analysis of P-CNTF and CSA-CNTF in terms of specific strength, specific modulus, electrical conductivity, thermal conductivity and ampacity.

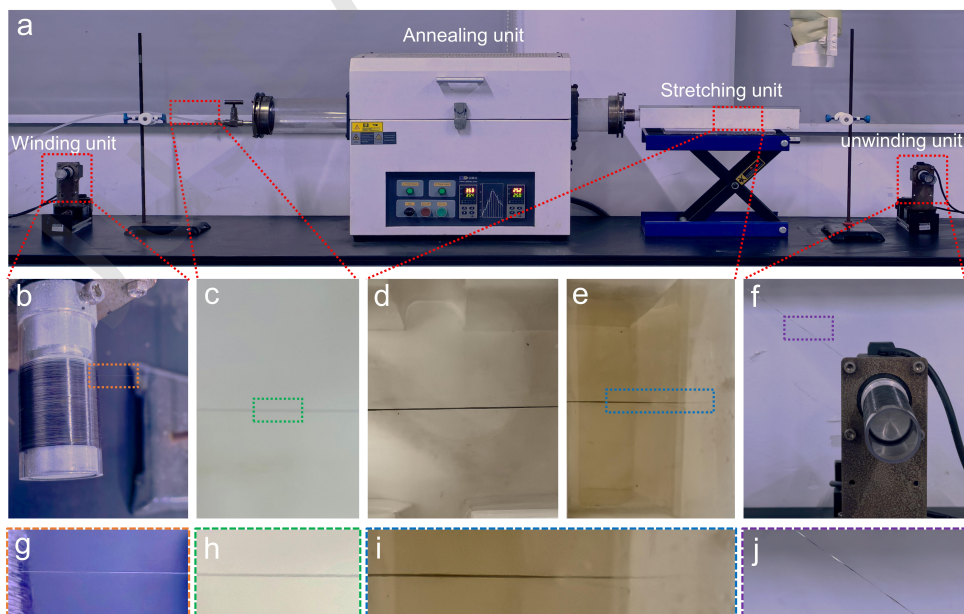


Figure S24. (a) CSA-assisted system for fiber stretching. (b-j) Photographs of CNTF during stretching process.

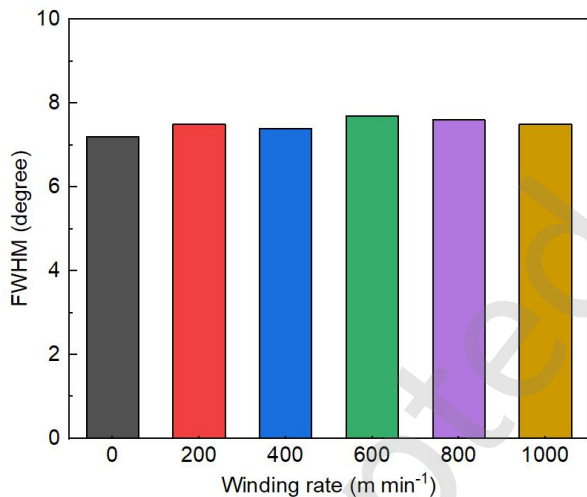


Figure S25. FWHM statistical analysis of WAXS patterns for scalable CSA-CNTF.

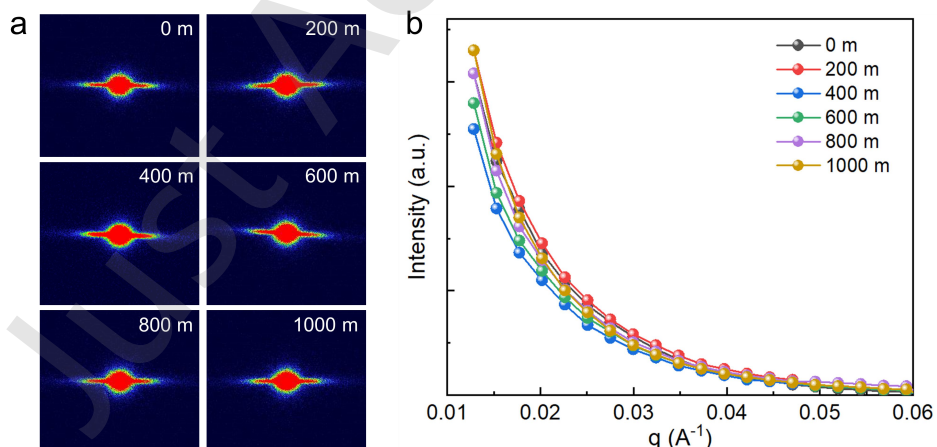


Figure S26. (a) SAXS patterns of scalable CSA-CNTF at different positions. (b) Scattering intensity of the fiber streak as a function of q along the equator for scalable CSA-CNTF at different positions.

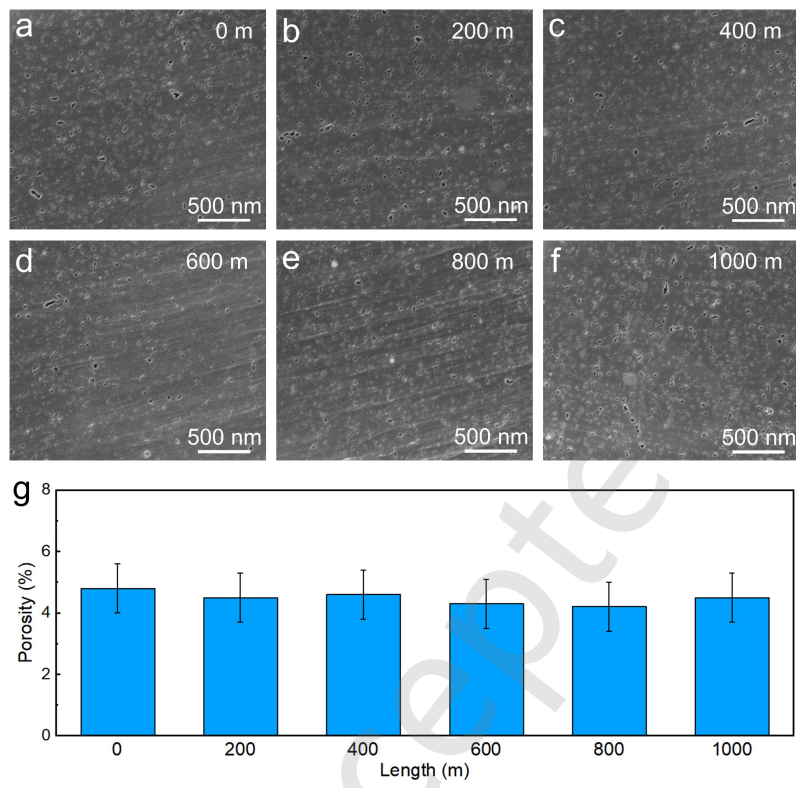


Figure S27. Cross-sectional SEM images (a-f) and porosity analysis (g) of scalable CSA-CNTF at different positions.

Supplementary Tables

Table S1. Comparison of CSA-CNTF and commercial fibers in terms of density, specific strength, specific modulus, electrical conductivity and thermal conductivity.

Materials	Density (g cm ⁻³)	Specific strength (N tex ⁻¹)	Specific modulus (N tex ⁻¹)	Specific conductivity (S m ² kg ⁻¹)	Thermal conductivity (W m ⁻¹ K ⁻¹)
This work	1.45±0.2	4.10±0.22	268±16	1480	400
T300	1.76	2.01	131	33.4	10.5
T700	1.80	2.72	128	34.7	9.6
T800	1.80	3.27	163	42.7	11.3
T1000	1.80	3.54	163	39.7	10.5
T1100	1.79	3.91	181	39.9	13
M35JB	1.75	2.69	196	51.9	38.9
M40JB	1.77	2.49	213	56.5	66.9
M46JB	1.84	2.28	237	60.4	83.6
M55JB	1.91	2.10	283	65.4	155.6
M60JB	1.93	1.98	305	74.0	150.5
K1352U	2.12	1.70	292	71.5	140
K1392U	2.15	1.72	353	93.0	210
K13C6U	2.18	1.65	413	229.4	580
K13D2U	2.2	1.68	425	303.0	800

Table S2. Comparison of CSA-CNTF and reported CNTFs in terms of method, specific strength and specific modulus.

Materials	Method	Specific strength (N tex ⁻¹)	Specific modulus (N tex ⁻¹)	Reference
CNTF	FCCVD spinning	4.10±0.22	268	This work
CNTF	FCCVD spinning	5.7±0.1	120±6.7	[S1]
CNTF	FCCVD spinning	4.62±0.24	134.82±12.16	[S2]
CNTF	FCCVD spinning	5.5±0.84	180±30	[S3]
CNTF	FCCVD spinning	5.5±0.2	211.4±14.6	[S4]
CNTF	FCCVD spinning	4.08±0.25	187.5 ± 7.4	[S5]
CNTF	FCCVD spinning	5.54	242	[S6]
CNTF	FCCVD spinning	5.8±0.42	174	[S7]
CNTF	FCCVD spinning	3.1	110	[S8]
CNTF	Wet spinning	3.43±0.26	186.87±27.93	[S9]
CNTF	Wet spinning	1.54	160	[S10]
CNTF	Wet spinning	3	209	[S11]
CNTF	Wet spinning	3.84	368	[S12]

References

- [S1] Zhang, X.;Lei, X.;Jia, X.;Sun, T.;Luo, J.;Xu, S.;Li, L.;Yan, D.;Shao, Y.;Yong, Z.;Zhang, Y.;Wu, X.;Gao, E.;Jian, M.; Zhang, J. Carbon nanotube fibers with dynamic strength up to 14 GPa. *Science* **2024**, *384*, 1318-1323.

- [S2] Hu, Z.;Sun, X.;Zhang, X.;Jia, X.;Feng, X.;Cui, M.;Gao, E.;Qian, L.;Gao, X.; Zhang, J. Kinetic Modulation of Carbon Nanotube Growth in Direct Spinning for High-Strength Carbon Nanotube Fibers. *Journal of the American Chemical Society* **2024**, *146*, 11432-11439.
- [S3] Oh, E.;Cho, H.;Kim, J.;Kim, J. E.;Yi, Y.;Choi, J.;Lee, H.;Im, Y. H.;Lee, K.-H.; Lee, W. J. Super-Strong Carbon Nanotube Fibers Achieved by Engineering Gas Flow and Postsynthesis Treatment. *ACS Applied Materials & Interfaces* **2020**, *12*, 13107-13115.
- [S4] Cho, Y. S.;Lee, J. W.;Kim, J.;Jung, Y.;Yang, S. J.; Park, C. R. Superstrong Carbon Nanotube Yarns by Developing Multiscale Bundle Structures on the Direct Spin-Line without Post-Treatment. *Advanced Science* **2023**, *10*.
- [S5] Lee, J.;Lee, D.-M.;Jung, Y.;Park, J.;Lee, H. S.;Kim, Y.-K.;Park, C. R.;Jeong, H. S.; Kim, S. M. Direct spinning and densification method for high-performance carbon nanotube fibers. *Nature Communications* **2019**, *10*.
- [S6] Shi, H. L.;Shi, Q. Q.;Zhan, H.;Ai, J. J.;Chen, Y. T.; Wang, J. N. High-Strength Carbon Nanotube Fibers from Purity Control by Atomized Catalytic Pyrolysis and Alignment Improvement by Continuous Large Prestraining. *Nano Letters* **2023**, *23*, 10739-10747.
- [S7] Wu, K.;Wang, B.;Niu, Y.;Wang, W.;Wu, C.;Zhou, T.;Chen, L.;Zhan,

X.;Wan, Z.;Wang, S.;Yang, Z.;Zhang, Y.;Zhang, L.;Zhang, Y.;Yong, Z.;Jian, M.; Li, Q. Carbon nanotube fibers with excellent mechanical and electrical properties by structural realigning and densification.

Nano Research **2023**, *16*, 12762-12771.

- [S8] Zhou, T.;Niu, Y.;Li, Z.;Li, H.;Yong, Z.;Wu, K.;Zhang, Y.; Li, Q. The synergetic relationship between the length and orientation of carbon nanotubes in direct spinning of high-strength carbon nanotube fibers. *Materials & Design* **2021**, *203*, 109557.
- [S9] Huang, J.;Guo, Y.;Lei, X.;Chen, B.;Hao, H.;Luo, J.;Sun, T.;Jian, M.;Gao, E.;Wu, X.;Ma, W.;Shao, Y.; Zhang, J. Fabricating Ultrastrong Carbon Nanotube Fibers via a Microwave Welding Interface. *Acs Nano* **2024**, *18*, 14377-14387.
- [S10] Tsentalovich, D. E.;Headrick, R. J.;Mirri, F.;Hao, J.;Behabtu, N.;Young, C. C.; Pasquali, M. Influence of carbon nanotube characteristics on macroscopic fiber properties. *ACS applied materials & interfaces* **2017**, *9*, 36189-36198.
- [S11] Kim, S. G.;Heo, S. J.;Kim, J.-G.;Kim, S.;Lee, D.;Kim, M.;Kim, N. D.;Kim, D.-Y.;Hwang, J. Y.;Chae, H. G.; Ku, B.-C. Ultrastrong Hybrid Fibers with Tunable Macromolecular Interfaces of Graphene Oxide and Carbon Nanotube for Multifunctional Applications. *Advanced Science* **2022**, *9*, 2203008.
- [S12] Lee, D.;Kim, S. G.;Hong, S.;Madrona, C.;Oh, Y.;Park, M.;Komatsu,

N.;Taylor, L. W.;Chung, B.; Kim, J. Ultrahigh strength, modulus, and conductivity of graphitic fibers by macromolecular coalescence.
Science advances **2022**, *8*, eabn0939.

Just Accepted